POLITECNICO
MILANO 1863

SCUOLA DI INGEGNERIA INDUSTRIALE
E DELL'INFORMAZIONE

Interference induced by NGSO constellations on GSO systems: investigating the dependence on the GSO link characteristics

Tesi di Laurea Magistrale in
Space Engineering - Ingegneria aerospaziale

Author: **Alexandre Bouleux**

Student ID: 985958
Advisor: Prof. Lorenzo Luini
Co-advisors: Enrico Polo
Academic Year: 2022-23

Abstract

In this thesis, the impact of the interference induced by NGSO constellations on GSO systems is studied. This effect is investigated through the ratio of desired power received over interfering power received (C/I ratio), with the use of its Complementary Cumulative Density Function (CCDF). Data on power received from both GSO-to-Earth and NGSO-to-Earth links is collected through simulation of the links over a period of one year. Link frequencies in the Ku and Ka bands give rise to the need of taking into account tropospheric effects, in particular rain attenuation. Various GSO link characteristics directly affect the power received through the rain attenuation experienced by the radiowave. This work studies how changes in GSO elevation angle, rain height, and link frequency affect the amount of interference perceived by the ground station, by comparing the CCDF curves of C/I for the various cases. Correlation analysis is then conducted between the rain attenuation affecting the GSO-to-Earth link, and the ones affecting NGSO-to-Earth links. This analysis is done at multiple avoidance angle thresholds, using both intensity plots as a visual method, and comparaisons of linear correlation coefficients.

Keywords: NGSO constellation, GSO, interference, elevation angle, frequency, correlation, rain attenuation

Abstract in lingua italiana

In questa tesi viene studiato l'impatto dell'interferenza indotta dalle costellazioni NGSO sui sistemi GSO. Questo effetto è analizzato attraverso il rapporto tra la potenza desiderata ricevuta e la potenza interferente ricevuta (rapporto C/I), con l'uso della Funzione di densità cumulativa complementare (CCDF). I dati sulla potenza ricevuta da entrambi i collegamenti GSO-Terra e NGSO-Terra sono raccolti attraverso la simulazione dei collegamenti per un periodo di un anno. Le frequenze dei collegamenti nelle bande Ku e Ka comportano la necessità di tenere conto degli effetti troposferici, in particolare dell'attenuazione da pioggia. Diverse caratteristiche dei collegamenti GSO influiscono direttamente sull'attenuazione da pioggia subita dalle onde radio. Questo lavoro studia come le variazioni dell'angolo di elevazione del GSO, dell'altezza della pioggia e della frequenza del collegamento influenzino la quantità d'interferenza percepita dalla stazione di terra, confrontando le curve CCDF di C/I per i vari casi. Viene quindi condotta un'analisi di correlazione tra l'attenuazione da pioggia che influisce sul collegamento GSO-Terra e quella che influisce sui collegamenti NGSO-Terra. L'analisi viene effettuata a diverse soglie di avoidance angle, utilizzando sia i grafici di intensità come metodo visivo, sia il confronto dei coefficienti di correlazione lineare.

Parole chiave: costellazioni NGSO, GSO, interferenza, angolo di elevazione, frequenza, correlazione, attenuazione da pioggia

Contents

Introduction

As the need for communications has grown in the past decades, satellite transmissions have become a key tool in telecommunication systems. Their ability to reach remote regions, without being constrained by terrain and ground infrastructure has proven crucial.

In 1965, Intelsat 1 was the first commercial satellite to be placed in geosynchronous orbit (GEO). The GEO is a circular orbit with an altitude of 35786 km above the Earth, and lies in the equatorial plane. This particular orbit has an interesting propriety : for an observer on Earth, any object on a GEO appears fixed in the sky. From a telecommunication standpoint, this means that an antenna pointing at a satellite in GEO would not need to change its orientation over time in order to get the best possible reception. Since then, the GEO has been a major target for several applications. Earth observation missions, as well as commercial and military communications payloads have been placed frequently at this altitude, and around 600 satellites are now listed on this orbit [1].

The GEO is not the only important orbit for space telecommunications. Medium earth orbits (MEOs), defined as orbits with an altitude between 2000km and 35786km, notably hosts geopositioning systems such as GPS or Galileo. Low earth orbits (LEOs), orbits with an altitude lower than 2000km, complete the picture, the LEO region being crowded with meteorologic, scientific as well as communication satellites. Any orbit that is not both circular and with an altitude of 35786km is considered a non-geosynchronous orbit (NGSO). Satellites using such orbits will not be static in the sky, and are not always visible. For some missions, especially scientific ones, intermittent coverage is acceptable, and the use of multiple ground stations is possible. However, for commercial communications, loss of transmission has to be avoided as much as possible. Therefore, increasing the number of satellites in systems, spacing them along the same orbit, or other orbits with different inclinations, is a common solution.

The use of satellite constellations has thus become significantly more common over the last years. Since 2015, the american company SpaceX has been developing and launching satellites for their Starlink constellation. The goal of Starlink is to provide internet access, and ultimately mobile phone coverage to areas with few or no telecommunication

infrastructures. This is achieved by the use of low and very low orbits. In addition, these orbits provide the lowest delay possible for communications. However, a lower orbit translates into less coverage for each individual satellite. This is compensated by the use of a massive number of satellites, making Starlink a so-called « megaconstellation » : as of early 2023, the 3300 Starlink satellites in orbit represented more than 70% of LEO objects weighing more than 100kg [2]. This number will certainly be growing in the coming years, as Starlink has announced aiming for a total of around 12000 satellites, and other companies have shown an interest in exploiting lower orbits for their aims.

This raise in the number of LEO satellites creates a few issues. As the lower frenquency bands (such as the L, S or C bands) cannot accomodate the new demands in bandwidth, designs tend to use higher frequencies. In particular, the Starlink constellation uses the Ku and Ka frequency bands, which are also commonly used by GEO satellites: thus, the NGSO to Earth link can induce interference on the GEO to Earth link, reducing the quality of the signal received by the ground station. Recommendations have been put in place to mitigate this phenomenom. For example, exclusion zones, where the LEO satellite cannot transmit, can be used to reduce the interference. However, outside of these zones, the transmissions of the constellation still have an effect on the reception of the GEO satellites transmissions. As a consequence, studying the interference from these LEO satellites on GEO to Earth transmissions is important to understand how existing links will be affected, and how to take these effects into account for future designs of GEO links. Given that GEO to Earth links can present various parameters, it is interesting to study how these varying link parameters affect the interference on the link.

The goal of this thesis is to study how the variations of the parameters of the GEO to Earth link will affect the interference created by LEO constellations, using a simulator taking into account tropospheric effects, specifically rain attenuation, to account for the high operational frequencies employed [3]. This work is structured as follows: Chapter 1 focuses on the models used throughout the work, as well as on the existing litterature on rain attenuation. Chapter 2 describes the simulator built to reproduce and study the scenario, together with its implementation and its usage. This section also addresses the validation of its rain attenuation model against existing models, (e.g. ITU-R recommandations). In Chapter 3, the variation in intereference caused by changes in elevation angle of the GSO link, rain height, link frequency and number of NGSO satellite considered is studied. This chapter will also discuss the correlation between GSO-to-Earth and NGSO-to-Earth rain attenuation, comparing existing correlation models with data from the simulator.

1 | Description of the models used

1.1. Description of models used

1.1.1. Spatial reference frame

Before studying Earth-space links, a reference frame has to be defined. For calculations on objects orbiting the Earth, a commonly used reference frame is the **Earth Centered Earth Fixed** (ECEF) one. Its origin is situated at the center of mass of the Earth, the z-axis goes through the North pole, the x-axis lies on the equatorial plane and goes through the Greenwich meridian, and the y-axis is orthogonal to both these axes, completing the right-hand reference frame. This reference frame translates and rotates with the Earth, making it a great tool to derive orbits, and calculate distances and line-of-sights between two points. However, the ECEF frame fails to consider that the Earth is not a perfect sphere, but an ellispsoidal object. This creates problems when trying to evaluate the position of points on the surface of the planet, or calculate distances between two of those points. A solution to this issue is to adopt the **Ellipsoidal Reference System**. In this frame, the positions of the points are defined by their latitude, longitude and altitude. The latitude is the angle between the point and the equatorial plane, the longitude the angle between the point and the reference planed defined by the Earth's rotation axis and the Greenwich meridian. The altitude is the height of the point above the Earth's surface. The shape of the surface is defined with a reference ellipsoids : the most broadly accepted one is the "WGS84", which is used, among other systems, by the Global Positioning System (GPS).

As coordinates can be easily converted between these two frames, both are used in communications : the ECEF is very practical when considering the positions of objects in space, whereas the Ellipsoidal Reference System finds its use when links between two positions are studied.

1.1.2. Kepler's laws and Keplerian elements

Orbits, whether those of artificial satellites or natural ones, are governed by a few physical principles, that need to be defined before studying the GSO and NGSO cases. This section aims to describe some of the orbital mechanics at play in the case we are interested in.

The system considered here consists of a satellite of mass m_s orbiting around the Earth, of mass m_e. As the system is far from any other massive celestial bodies, and the masses of nearby satellites are negligible compared to the mass of the Earth, it is possible to reduce this problem to a **two-body problem**. Furthermore, as $m_s << m_e$, the gravitational force of the satellite does not affect the movement of the Earth. Thus, the problem is further simplified to a **restricted two-body problem**. In this context, *Kepler's Laws* apply, and in the case of an articial satellite, can be expressed as follows [4] :

- **First law** : the orbit of a satellite around the Earth describes an ellipse, with the Earth positioned at one of the two foci, as shown in Figure 1.1.
- **Second law** : a segment drawn between the satellite and the Earth, sweeps equal areas of space during equal lengths of time, as the satellite moves along its orbit.
- **Third law** : the square of a satellite's orbital period is proportional to the cube of the semi-major axis of its orbit.

Kepler's first law indicates that the shape of the orbit is an ellipse. The ellipse is mathematically described by the equation :

$$r = \frac{p}{1 + e\ cos\ \nu} \tag{1.1}$$

with r the distance between the satellite and the Earth, p the *semi-latus rectum* of the ellipse, e its **eccentricity** and ν the **true anomaly** of the spacecraft.

The eccentricity e and the true anomaly ν are two of the six **Keplerian elements** that describe the characteristics of an orbit and the position of the satellite along it. The eccentricity describes the shape of the ellipse, in particular its oblateness, and is comprised between 0 and 1. An eccentricity of 0 means the ellipse is a circle, an eccentricity of 1 or higher describes an hyperbola. The true anomaly defines the position of the spacecraft alongs its orbit. It is the angle between the Earth-perigee direction (the perigee being the point of the orbit closest to the Earth) and the current Earth-satellite direction. The other Keplerian elements are :

- the **semi-major axis**, a, is defined as half of the length of the major axis of the

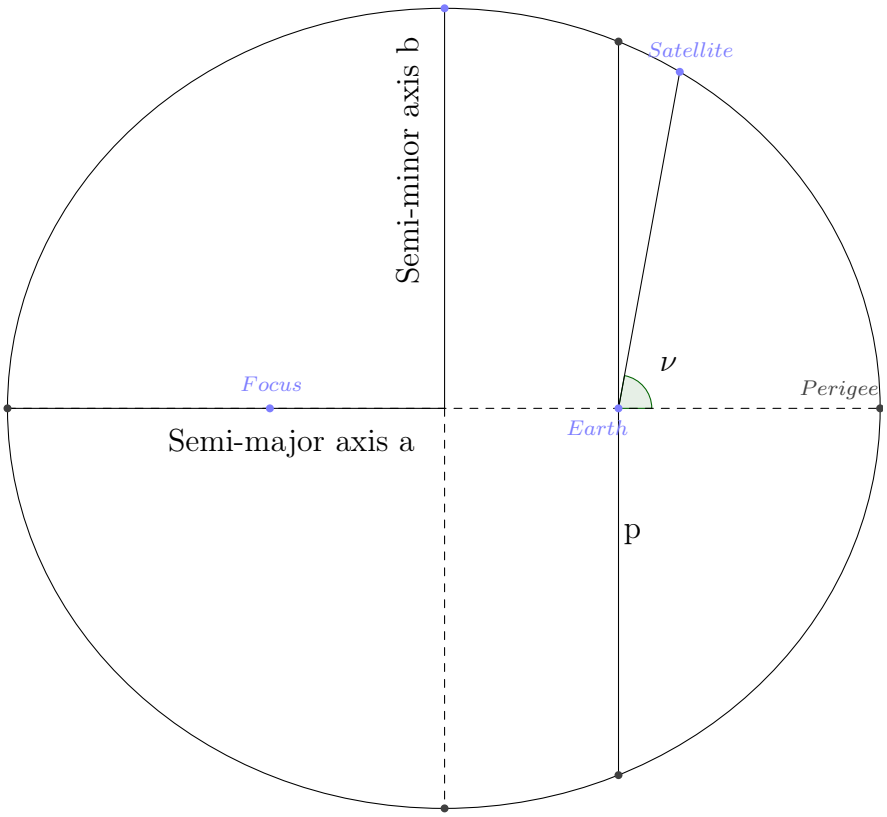

Figure 1.1: Orbit of a satellite around the Earth, viewed normal to the orbital plane.

ellipse. It is linked to the semi-latus rectum by the expression $p = a(1 - e^2)$.

- the **inclination**, i, is the angle between the orbital plane, and a reference plane. In the case of an orbit around the Earth, the reference plane is usually the equatorial plane.
- the **right ascension of the ascending node**, Ω. It is the angle between the *vernal direction* (the Earth-sun direction at the time of the March equinox) and the Earth-ascending node direction. The ascending node is the point at which the orbit crosses the reference plane, going from the southern hemisphere to the northern hemisphere.
- the **argument of the perigee**, ω, is the angle on the orbit plane between the Earth-ascending node direction and the Earth-perigee direction.

These Keplerian elements completely define an orbit : a unique set of these elements exists for every orbit. They can be used to derive the complete motion of a satellite around the Earth, and can be transcribed to cartesian coordinates.

Kepler's second law is useful to understand that the satellite does not move at a constant speed along its orbit. It moves faster the closer to the perigee, and slower the closer to the apogee.

Kepler's third law creates a relation between the semi-major axis of the orbit, and the orbital period. Its exact mathematical expression is :

$$T^2 = \frac{4\pi^2}{\mu} a^3 \tag{1.2}$$

with T the period of the orbit in s, a the semi-major axis of the orbit in km, and μ, in our case, the **geocentric gravitational constant**. It is defined as $\mu = GM_E$, with G the universal gravitational constant, and M_E the mass of the Earth. The value of μ is $398600 km^3/s^2$. In the case of a circular orbit ($e = 0$), the radius r of the orbit is equal to its semi-major axis a. Therefore, from Equation 1.1.3, the radius can be expressed as :

$$r = (\frac{\mu}{4\pi^2})^{\frac{1}{3}} T^{\frac{2}{3}} \tag{1.3}$$

When given an orbital period, it is thus possible to find the radius of the circular orbit that has this period : this is a key result for the design of space systems, as this allows to find the required altitude for the purpose of the satellite.

1.1.3. Geostationary and non-geostationary orbits

Equation 1.1.3 links orbital period and orbit semi-major axis. One period is of particular interest for the design of space telecommunication systems : it is the period of rotation of the Earth on its axis, also known as the **sidereal day**. This period is approximatively 23 hours 56 minutes and 4 seconds, or 86164 seconds. With this data and Equation , the semi-major axis of this orbit is calculated as the following :

$$r = \left(\frac{398600}{4\pi^2}\right)^{\frac{1}{3}} 86164^{\frac{2}{3}} = 42164\ km \tag{1.4}$$

Any orbit with this semi-major axis is called a **geosynchrous orbit** (GSO). From the viewpoint of an observer on Earth, a satellite on a GSO returns to the same point in the sky each sidereal day. Moreover, a GSO with the added assumptions that the orbit is circular ($e = 0$), and situated on the equatorial plane ($i = 0$) is a **geostationary orbit**(GEO). This orbit has an important particularity for the telecommunication systems : any object on the geostationary orbit appears fixed in the sky when seen from the Earth. Therefore, an antenna pointing at a satellite in GEO requires very little pointing corrections over time in order to operate. A spacecraft at such altitude (35786 km from the surface of the Earth), also sees about one third of the surface of the Earth, meaning that complete coverage of the planet can be achieved with only three satellites.

However, the delay in the transmission created by the distance over which the wave has to travel, the important path losses, and limited number of satellites that can be placed on this orbit, mean that other orbits have to be used for purposes that do not require a geostationary satellite.

These orbits are called **non-geosynchronous orbits** (NGSO). The usual NGSO orbits are **Low Earth Orbits** (LEO), **Medium Earth Orbits** (MEO) and **Highly Elliptical Orbits** (HEO). Low Earth Orbits, are orbits with an altitude up to 2000km. Satellites on low orbits suffer from less transmission delay and path losses than GEO satellites, but cover way less of the Earth's surface and are only above the horizon, and thus visible, only a few minutes at a time. Therefore, to obtain complete coverage, multiple spacecraft are used. A space system that consists of a group of satellites on the same orbit is a **constellation**.

Medium Earth Orbits are any orbits with an altitude between 2000km and the GSO altitude. With a delay higher than for LEO satellites, but a larger coverage, they are mostly used for meteorology and positioning systems such as *GPS*.

Highly Elliptical Orbits are orbits with a high eccentricity. HEOs are interesting to reach latitudes that other orbits struggle to cover, and they can also provide extended time coverage to specific zones. For example, HEO are particularly suited for polar observations missions.

1.1.4. Rain attenuation

As satellites using the Ka and Ku bands are studied, it is necessary to investigate the consequences of rain attenuation on communications. In fact, for frequencies above 10GHz, the effect of rain is the most important perturbation for radio transmissions [5]. This is caused by the wavelength of a signal with this frequency approaching the size of rain drops (from tenths of millileters to a few millimeters), and thus being affected the most by this perturbation. Rain attenuation is caused by two physical phenomena : absorption and scattering of the radio wave. Its impact depends on multiple parameters, some related to the rainfall (rain rate, drop size distribution), some to the link (frequency, elevation angle, wave polarization). To calculate rain attenuation, two assumptions on the propagation of the wave and on the rainfall are considered :

- The rain drops are assumed to be spherical, and to absorb and scatter energy from the radio wave. Depolarization effects are not considered.
- The contributions of each drop are additive and independent from other drops (single scattering assumption).

The attenuation of a radio wave that propagates through rain, along a path of length L, can be expressed as :

$$A = \int_L \gamma_R \, dx \tag{1.5}$$

where γ_r is the specific attenuation, in dB/km [6].

Geometry of a rain event

To derive the rain attenuation on a wave, one needs to determine the length of its path through the rain. For this, an investigation the geometry of the link compared to the structure of precipitations has to be conducted. As shown in Figure 1.2, a rain event is characterized by three distinct zones, separated vertically.

- Zone A is an area of **liquid precipitation**. Up until the altitude of the 0°C isotherm, the water is in a liquid state. Although the rain rate can vary dramatically

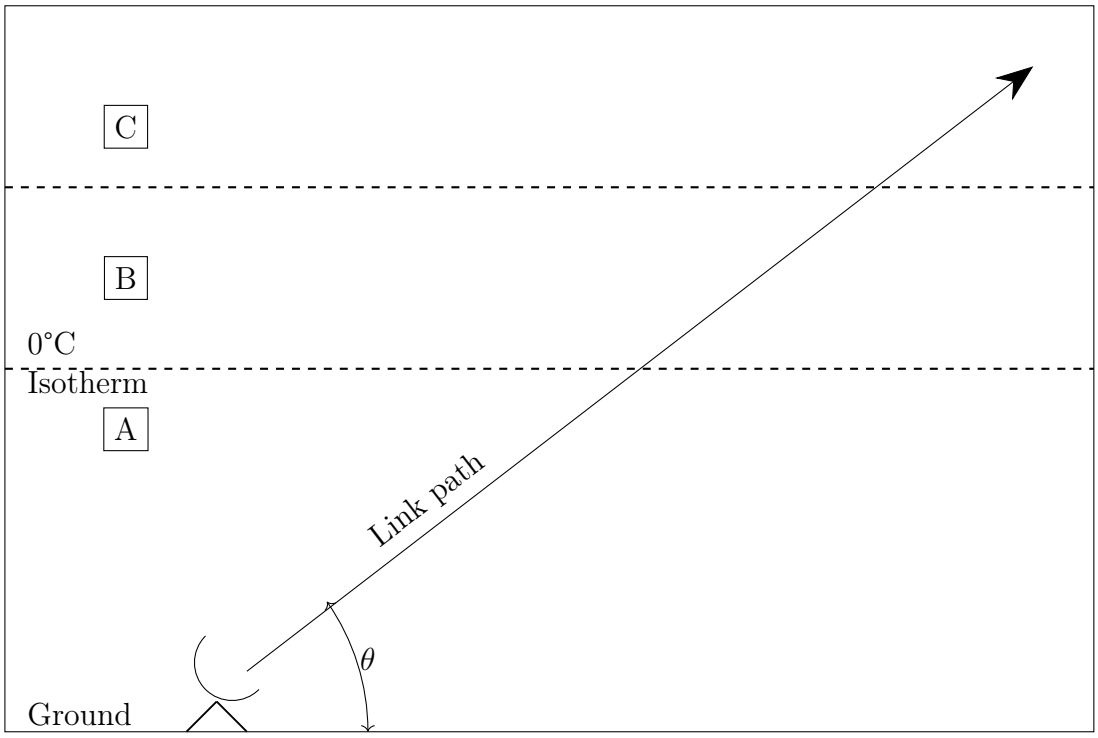

Figure 1.2: Geometry of a ground-to-space radio transmission through a rain event.

on the horizontal axis, it is about constant on the vertical axis.

- Zone B is the **melting layer**. Just above the 0°C isotherm line, water takes the form of a mix of snow and liquid water. As the particles in this region behave like large rain drops seen by the radio wave, it has to be taken into account for the derivation of attenuation. This is normally done in an effective way by increasing the actual rain height.
- Zone C is an area of **frozen particles**. Above the melting layer, all of the water is in a solid state. As ice tends to be transparent to radio waves, at least until 70GHz, the attenuation it creates on the link can be neglected.

To take into account the attenuation caused by the melting layer, the rain height h_r is defined as the equivalent height of the liquid precipitation zone, with the width of the melting layer reduced to 0, and keeping the same attenuation. Recommendation ITU-R P.839-4 describes the rain height as 0.36km above the altitude of the 0° isotherm, to account for the melting layer [7]. With this, a simplified geometry of the event is obtained, as shown in Figure 1.3.

With this, the length of the slant-path L is finally defined, as the length of path that the

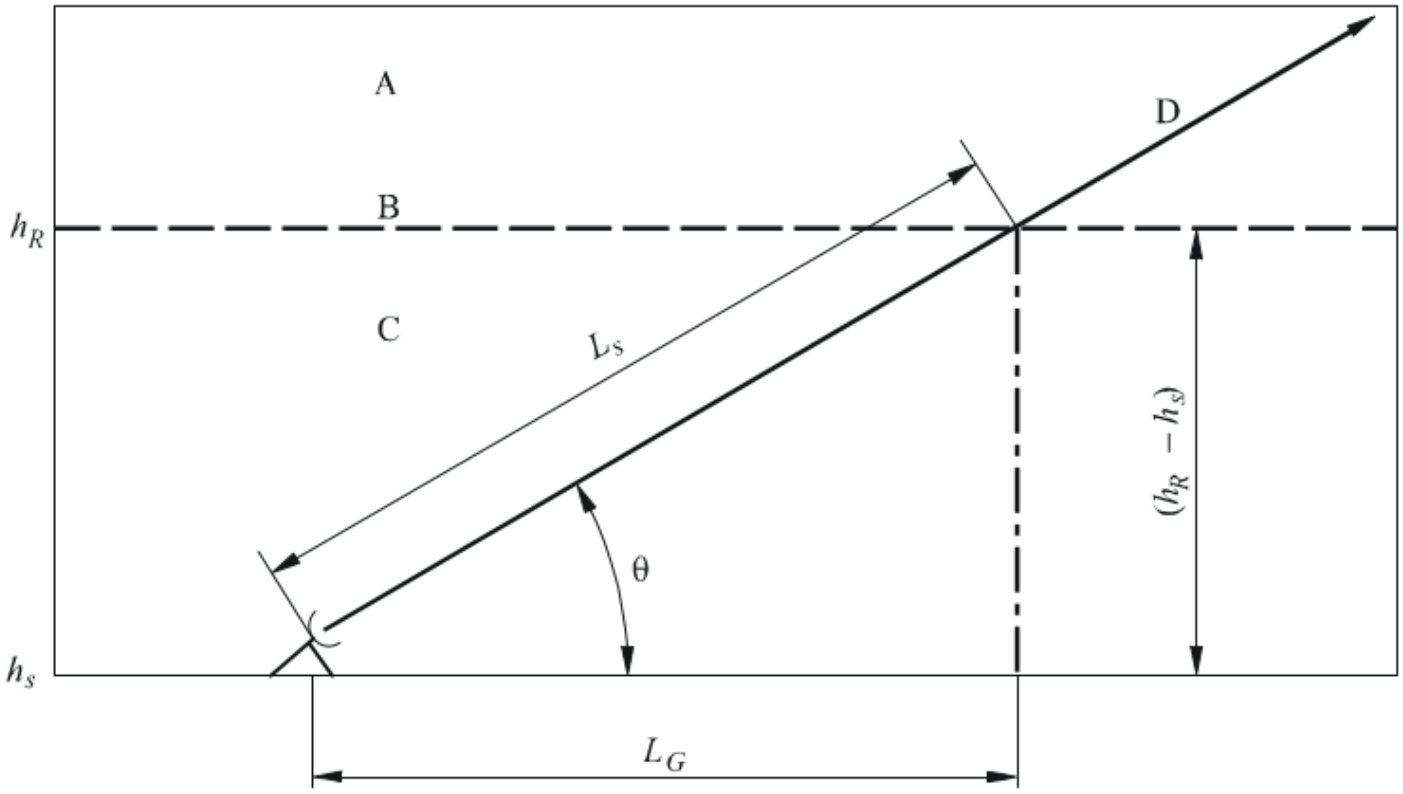

Figure 1.3: Satellite transmission during a rain event, with rain height as descibed in ITU-R Recommandation P.839-4. (Source: ITU-R Recommendation P.618-14 [8])

wave takes under the rain height. Geometrically, L is described as such:

$$L = \frac{(h_r - h_s)}{sin\theta} \tag{1.6}$$

with θ being the **elevation angle** of the link.

Calculation of the specific attenuation using ITU-R Recommendation P.838-3

In Recommendation P.838-3, the ITU-R recommends using the following expression to calculate the specific attenuation [6]:

$$\gamma_R = aR^b \tag{1.7}$$

with R the rain rate in mm/h, and a and b coefficients that are function of the frequency. If the polarization of the wave is either horizontal or vertical, these coefficients are calculated

using the following equations :

$$log_{10}a = \sum_{j=1}^{4} \left(a_j exp \left[- \left(\frac{log_{10}f - b_j}{c_j} \right)^2 \right] \right) + m_a log_{10}f + c_a \tag{1.8}$$

$$b = \sum_{j=1}^{5} \left(a_j exp \left[- \left(\frac{log_{10}f - b_j}{c_j} \right)^2 \right] \right) + m_b log_{10}f + c_b \tag{1.9}$$

The coefficients a_j, b_j, c_j, m_a, m_b, c_a, c_b are tabulated in Recommendation ITU-R P.838-3, and depend on the wave polarization and frequency. For linear and circular polarization, a and b can be calculated with these equations :

$$a = \frac{a_H + a_V + (a_H - a_V)\ cos^2(\theta)\ cos(2\tau)}{2} \tag{1.10}$$

$$b = \frac{a_H b_H + a_V b_V + (a_H b_H - a_V b_V)\ cos^2(\theta)\ cos(2\tau)}{2k} \tag{1.11}$$

a_H, b_H, a_V and b_V are the a and b coefficients for horizontal and vertical polarizations respectively, θ is the elevation angle, and τ the polarization tilt angle measured from the horizontal, taking 45° for a circular polarization.

1.1.5. EXCELL, MultiEXCELL and ST MultiEXCELL

The calculation of rain attenuation necessitates the knowledge of the rain rate along the path of the transmission. To obtain this information, mathematical models are used to simulate the structure of rainfall, and in particular the structures of rain cells. Rain cells are defined as geographical zones inside of which the rain rate exceeds a certain value. In 1987, the *EXCELL* model was developed from radar measurement of real rain cells [9]. *EXCELL* provides a model of the horizontal distribution of rain rate for one rain cell, based on an exponential shape. It also provides an algorithm to find the probability of occurence for a cell at any given site, given the measured complementary cumulative distribution function (CCDF) of the rain rate. However, *EXCELL* is limited to one rain cell, meaning that the scale on which it can be used for attenuation calculation has to be small.

Addressing this issue, the *MultiEXCELL* model was presented in 2011 [10]. This model has been developed from weather measurements made with the weather radar in Spino d'Adda, near Milan, Italy. Besides describing the structure and parameters of single rain cells, it is also able to describe the spatial features of a rain field on a larger scale. To achieve this, it looks into how the rain cells regroup into clusters, studying the number of

cells in clusters, the distance between those cells, and the distance between the clusters throughout the rain field. Furthermore, it studies an important parameter for the spatial correlation of rainfall : the fractional area of the map that is covered by rain, η_p, which is also derived from the radar data. *MultiEXCELL* is thus able to output rain maps with satisfactory spatial correlation; however, it does not describe the evolution of the system over time.

In order to derive the time correlation of the rain system, the *ST-MultiEXCELL* model was developed, and presented in 2020 [11]. The evolution over time of the system is derived by considering the changes in structure of the rain cells and their movement over the field, and incorporating the evolution of the fractional area covered by rain η_p. For this, a realistic time evolution of η_p is considered, relying on data from Numerical Weather Prediction datasets, in particular the ERA40 database. A first *MultiEXCELL* rain map is generated, then each cell is identified, and truncated at 0.5 mm/h. The structural evolution of the cells is derived using the location of the site, as well as the evolution of η_p. The rain cells are displaced with a velocity v and a direction θ, calculated from values of the wind intensity and direction. The map for the next time step is generated, and the process repeats until the event is over. As the data in the ERA40 is presented in 6 hours timeslots, *ST-MultiEXCELL* outputs 6 hours long events, with a time resolution of 1 minute. The data consists of 200km $\times$ 200km maps, with each pixel of 1km $\times$ 1km containing the rain rate in its area in mm/h. A graphical representation of a typical map produced by *ST-MultiEXCELL* is shown in Figure 1.4. Compared with data from the Spino d'Adda site, *ST-MultiEXCELL* has shown to output sufficiently realistic rain maps for use in wave propagation simulations.

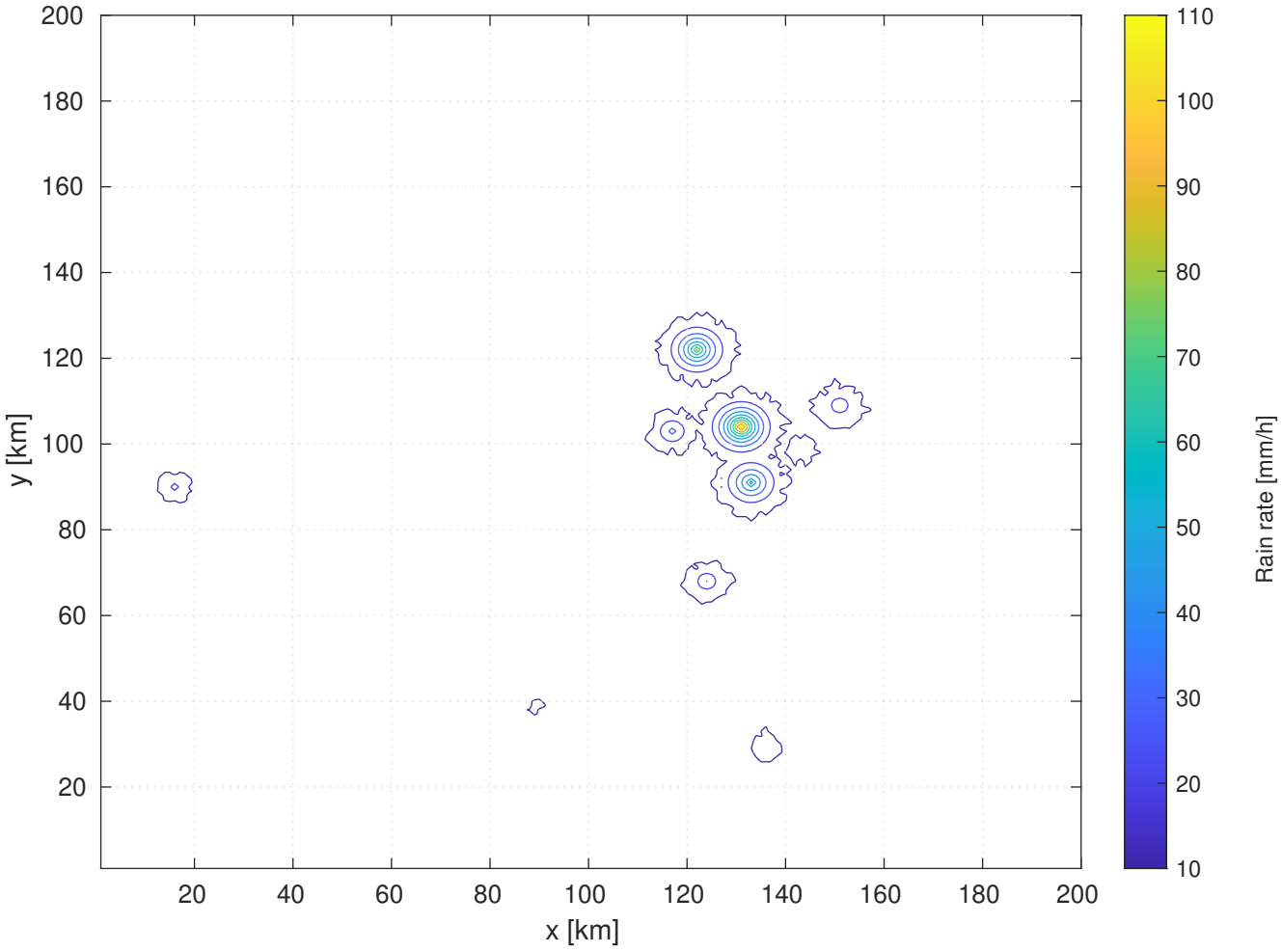

Figure 1.4: Contour plot of a rain map generated by ST-MultiEXCELL, at a fixed time.

2 | Description of the simulator

2.1. Aim of the simulator

2.1.1. Measuring the interference induced by VLEO constellations

The number of spacecrafts in Very Low Earth Orbits (VLEO) constellations has been rapidly growing over the last years, and should keep growing in the near future. These satellites have the peculiarity of generally emitting on the same bands as GSO satellites: this induces interference between the signals, as the ground station of the GSO system can receive the transmissions coming from the NGSO spacecrafts. Even though regulations have been put in place to mitigate the issue, it remains an important problem for the functioning of current geostationary systems, as well as for the design of future ones.

In 2022, this motivated the creation of a model implemented by software, with the aim of evaluating these inteferences by simulating the GSO and NGSO links over a period of one year [3]. One metric used by this work to quantify interference is the **C/I ratio**. This value is the ratio of the power received from the signal of the desired link, i.e. the GSO one, over the power received from the interfering links, i.e. the transmissions of the NGSO spacecrafts. Its expression is as follows :

$$C/I = 10log_{10}\left(\frac{P_{rx,GSO}[W]}{\sum_{i=1}^{Nco} P_{rx,NGSO,i}[W]}\right) \quad [dB] \tag{2.1}$$

$P_{rx,GSO}$ is the power received at the ground station from the GSO link, and $P_{rx,NGSO,i}$ the power received at the ground station from one NGSO spacecraft i, while Nco is the number of maximum NGSO satellites allowed to transmit and thus contributing to the interference. As the receiver perceives several NGSO transmissions, the total interfering power is the sum in Watts of all interfering powers, as the signals emitted by each NGSO satellites are assumed to be independent.

This thesis uses this simulator extensively : as such, the following sections aim at detailing

its workflow.

2.1.2. Evaluation of power budget

In order to calculate the C/I ratio for every time step, it is necessary to obtain the power received at the earth antenna for both the GSO and NGSO, i.e. their **power budget**. The expressions used by the simulator to derive them are presented in this section.

The power budget of the GSO link is evaluated as follows :

$$P_{rx,GSO} = EIRP \ + \ G_{rx} \ - \ fsl_{GSO} \ - \ Att_{rain,GSO} \qquad [dBW] \tag{2.2}$$

with $EIRP$ being the effective isotropic radiated power of the GSO satellite in dbW, G_{rx} the gain of the receiving antenna in dBi, fsl_{GSO} the **free space losses** along the link, and $Att_{rain,GSO}$ the attenuation caused by rain on the GSO link, the calculation of which is described in Section 2.3.2. The free space losses are calculated as follows :

$$fsl_{GSO} = 20log(\frac{4\pi d}{\lambda}) \qquad [dB] \tag{2.3}$$

with d being the distance between the GSO satellite and the receiver, and λ the wavelength of the transmission.

As for the power budget of the NGSO link, the known value for the power transmitted by the satellite is the power flux density, which is a power for a unit surface. Thus, calculating the power at the receiver requires knowledge of the **effective area of the antenna**, A_{eff}.

$$A_{eff} = 10log_{10}\left(\frac{G_{rx}\lambda^2}{4\pi}\right) \qquad [dB(m^2)] \tag{2.4}$$

The power received by the antenna on the NGSO link is then :

$$P_{rx,NGSO} = PFD \ + \ A_{eff} \ - \ Att_{rain,NGSO} \qquad [dBW] \tag{2.5}$$

2.2. Parameters initialization and inputs

To calculate the power budget of both signals throughout one year of simulations, the simulator requires data about the links, as well as propagation conditions. This section details these inputs.

Table 2.1: Table of SpaceX VLEO constellation's orbital parameters. Source : Table A.2-2 [12]

Altitude	345.6 km	340.8 km	335.9 km
Number of satellites	2547	2478	2493
Orbital Inclination	53°	48°	42°

2.2.1. Positional data

The position of the ground station, as well as the position of the transmitting satellites over time are needed to determine the attenuation on both links. Thus, the simulator takes as input :

- the latitude, longitude and altitude of the ground station. For all future calculations done in this work, the ground station is situated in Spino d'Adda, close to Milan. Its coordinates are latitude of 45.4°N, longitude of 9.5°E and altitude of 0.084km.
- the latitude, longitude and altitude of the GSO satellite. As all satellite considered are on the GEO, their latitude is always 0°, and their altitude 35786km. Their longitude is chosen to provide a GSO link elevation angle as close as possible to the desired elevation angle, and is pulled from a list of currently employed GEO satellites.
- the orbital data of an NGSO constellation, as the evolution of their latitude, longitude and altitude in time. This work uses SpaceX Starlink very low Earth orbit (VLEO) constellation. This constellation is constituted of three groups of satellites on three different orbits. Their orbital parameters are presented in Table 2.1. The data consist of discrete geodetic coordinates with a time resolution of 30 seconds, the whole data set representing 5 days of orbit. This information has been provided by *SES S.A.*. To generate a full year of results, the evolution of the constellation over these 5 days is cycled. Their orbital parameters of note are described in Table 2.1.

2.2.2. Signal-related data

The derivation of the power budget necessitates the knowledge of several parameters linked to the power emitted by the satellites, as well as the configuration of the antenna. For the GSO satellite, the information is pulled from Resolution 770 of the ITU-R [13]. In particular, for the space-to-Earth downlink, the parameters are :

- EIRP density : 36 $[\frac{dBW}{MHz}]$

- Bandwidth : 1 MHz

The NGSO spacecrafts in the Starlink constellation studied adjust their emitted power depending on their steer angle, in order to maintain a constant Power Flux Density (PFD) on the ground. Thus, the parameter used by the simulator is the PFD of the link : -105.72 dB(W/m²/1MHz) [12]. The bandwidth for the NGSO transmission is also 1 MHz.

The antenna is modeled after an antenna manufactured by ©*CPI Vertex Antennentechnik GmbH*, and with a radiation pattern prescribed in Resolution P580-6 of the ITU-R [14]. Its maximum receive gain is $G_{rx} = 59.6dBi$.

2.2.3. Rain-related data

For the calculation of rain attenuation, two inputs are used : rain height and rain maps. Their usage will be discussed in Section 2.3.2. The rain height is either entered manually, or derived from the coordinates of the ground station by the use of the model described in recommendation P.839-4 of the ITU-R [7].

For rain rates, the data is supplied to the simulator under the form of rain maps. Rain maps are generated using *ST-MultiEXCELL* [11], and take the form of 200 × 200 matrices of rain rate in mm/h, that are generated with a time resolution of 1 minute. Each event generated by *ST-MultiExcell* lasts 6 hours, and thus comprises 359 rain maps. In order to achieve a finer resolution, the simulator interpolates every rain map with the next one, to form an intermediary matrix. The simulator thus has a temporal resolution of 30 seconds, or 717 time stamps per event. To cover a whole year worth of calculation, the simulator uses 1460 of these events. This includes clear-sky events, in which there is no rainfall.

2.3. Workflow of the simulator

2.3.1. Initialization phase

Before starting the iterations over rain maps, some constants are initialized during the first phase of the runtime.

- The rain height is either calculated as described in ITU-R P.839-4, or set as a specific fixed value.
- The geodetic coordinates of both the GSO satellite and the Earth station are used to find the azimuth, elevation angle and length of the GSO links, for use in attenuation calculation.

- The a and b parameters used for the calculation of specific rain attenuation in ITU-R Recommendation P.838-3 are derived.

The other purpose of the initialization phase is to determine which NGSO satellites are interfering with the GSO link throughout of the simulation. To do so, the model makes use of one of the most prevalent methods of mitigating NGSO on GSO-link interference : the use of the **avoidance angle**. This method is part of an ensemble of regulations, that impose coordination between operators in order to limit the power received by GSO receivers from NGSO transmissions [15] [16]. When the **separation angle**, ϕ, which is the angle between the GSO-Earth link and the NGSO-Earth link, is below a certain threshold α, the avoidance angle, the NGSO satellite ceases to emit. A graphical representation of this method is shown in Figure 2.1.

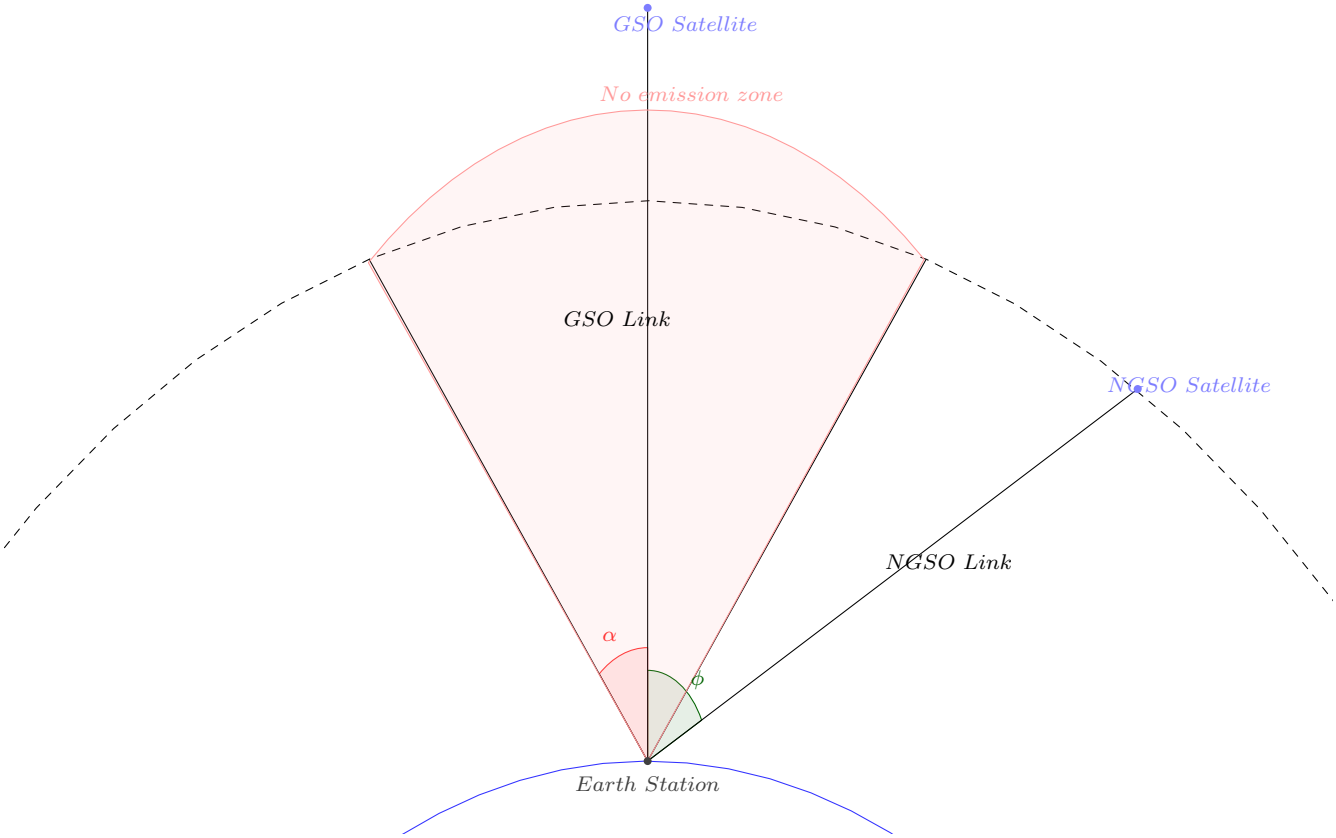

Figure 2.1: Graphical representation of avoidance angle method.

However, this phase filters out satellites in other ways : NGSO spacecrafts can only be interfering when they are visible. This is defined as the satellite having an elevation over 5°. Furthermore, the simulator can choose to retain only a select number of VLEO satellites to be interfering: this is another method found in regulations. This number is called the *Nco*. For exemple, with an Nco of 10, only 10 NGSO satellites will be considered

as interfering, and only these 10 power budgets will be calculated. The satellites can be either choosen at random throughout all the visible spacecrafts, or taken as the closest from the GSO link, with a separation angle above α. Finally, the azimuth, elevation angle, a and b parameters, and distance between NGSO satellite and Earth station are stored for the whole length of the simulation. The iteration can then begin.

2.3.2. Calculation of rain attenuation

As the frequency of the transmission is in the 20 to 40GHz range, the attenuation caused by the rain is preponderant in the total attenuation on the link. The simulator has a specific way of evaluating it for each time step, that is detailed here. Rain attenuation is calculated with the same method for both the GEO satellite, and all of the interfering NGSO spacecrafts.

At initialization of the simulator, the coefficients a and b for the calculation of specific attenuation are calculated using the method described in Section 1.1.4. As these coefficients only depend on the frequency, elevation angle and wave polarization, they are constant over the whole simulation for the GSO link. For each 30 seconds timestep, a rain map containing the rain rate is evaluated. With this, a 200km $\times$ 200km map of the specific attenuation, with resolution 1km $\times$ 1km, γ_R, is generated using Equation 1.7 on each pixel of the rain map. The specific attenuation map is a matrix of size 200 $\times$ 200, containing the value of γ_R in dB/km, for each square kilometer covered by the map.

Once the specific attenuation is evaluated, the next step is to integrate it over the whole path of the transmission in the rain, according to Equation 1.5. This calculation is done by considering the projection on the ground L_G of the slant path L. This segment has one extremity placed at the center of the map, the ground station, (x_0, y_0). The coordinates of the other end, (x_f, y_f), are found by first considering that the path points straight north, giving the coordinates (x_n,y_n),and then rotating the path clockwise by the azimuth, ψ, of the satellite. A graphical representation of this method is shown in Figure 2.2.

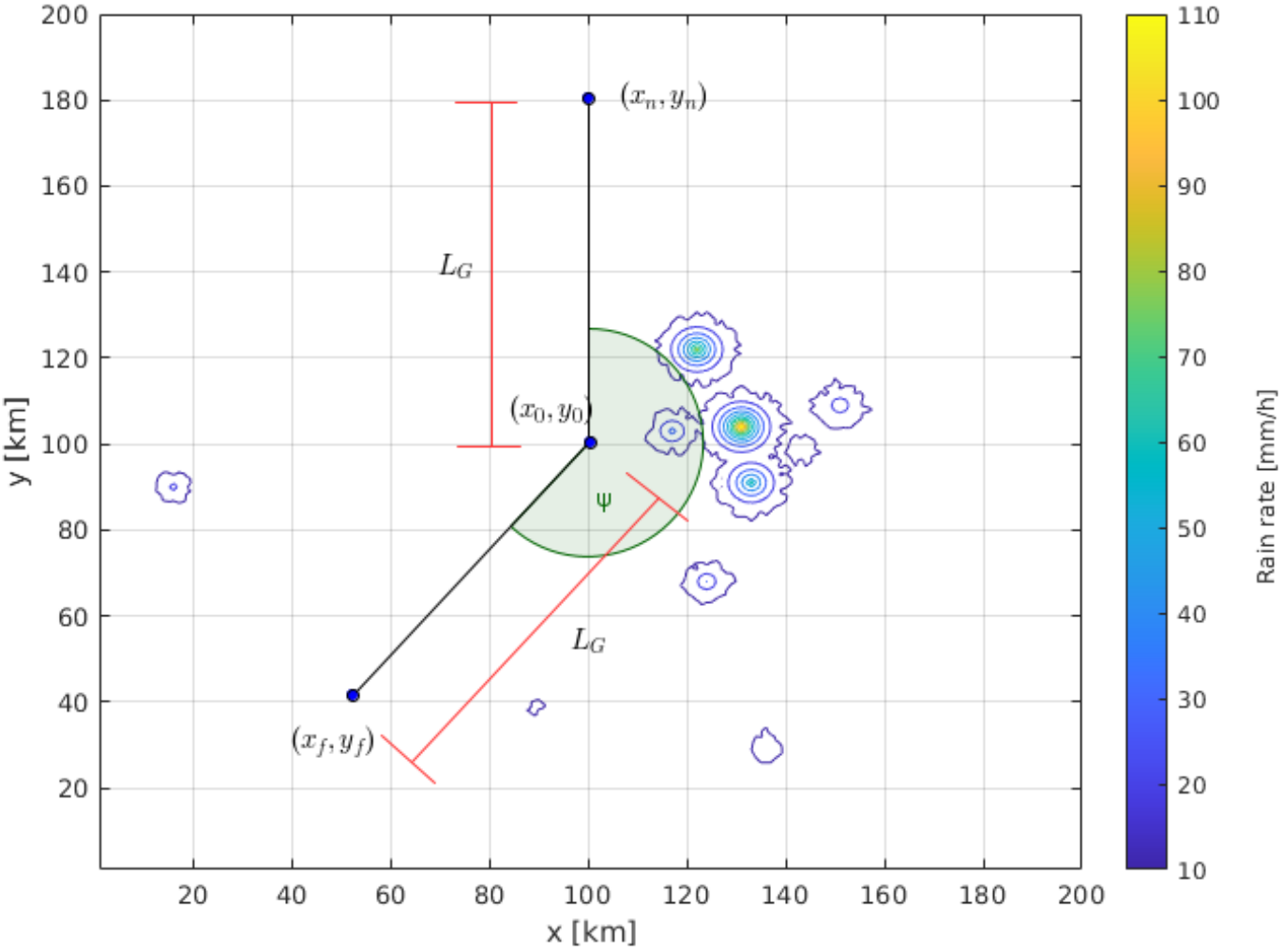

Figure 2.2: Top-down view of the method used to find the coordinates of the ground path.

Once this is done, and the complete ground path is evaluated, the simulator finds the intersections of L_G with the grid of specific attenuation map. The medium point between each intersection is found (as shown in Figure 2.3) : this determines which pixels of the map are actually crossed by the ground path. with this, the simulator creates a distance matrix, Δ_x, that contains the distance traveled by the ground path in each pixel of the map. Figure 2.4 shows the non-zero values of one such distance matrix.

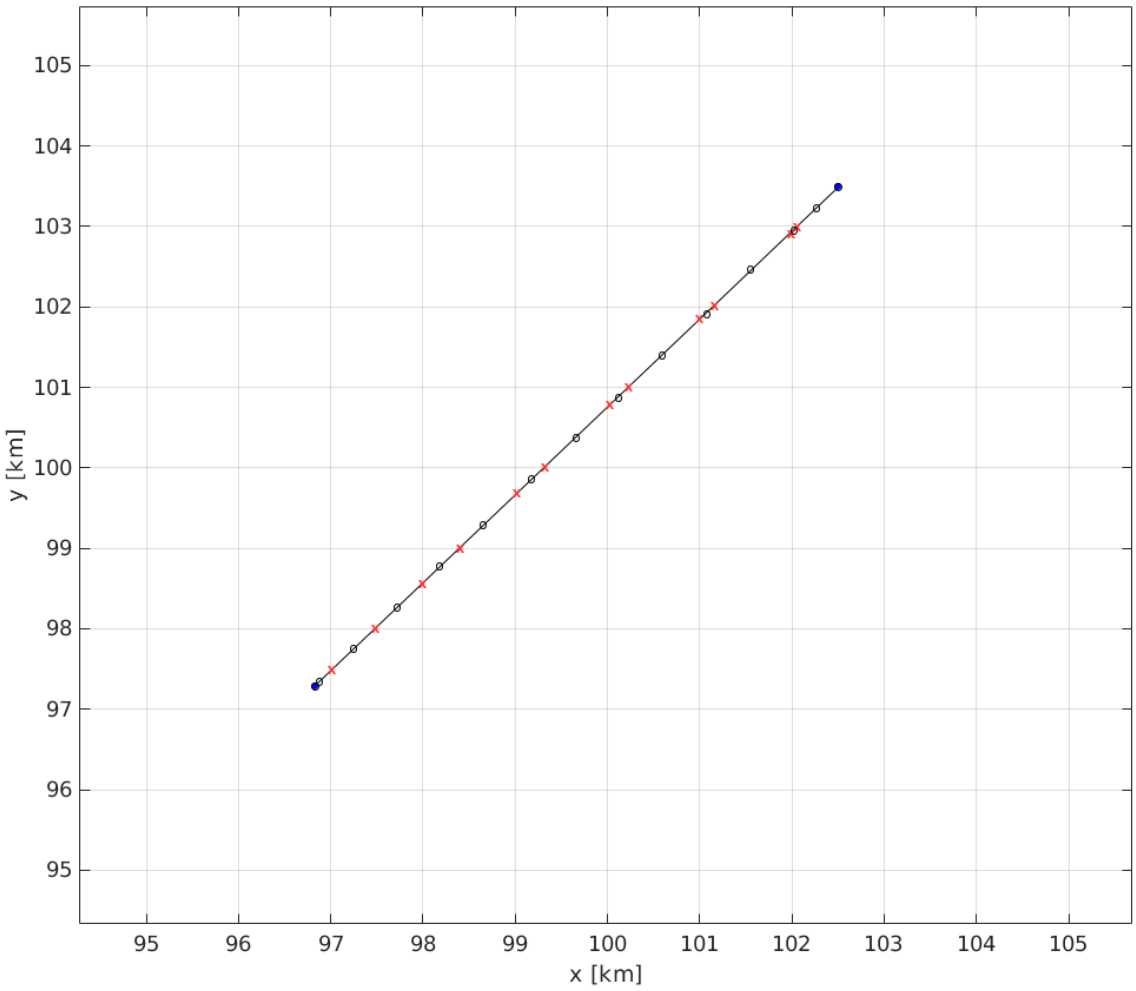

Figure 2.3: Ground projection of a slant path and its intersections with the grid.

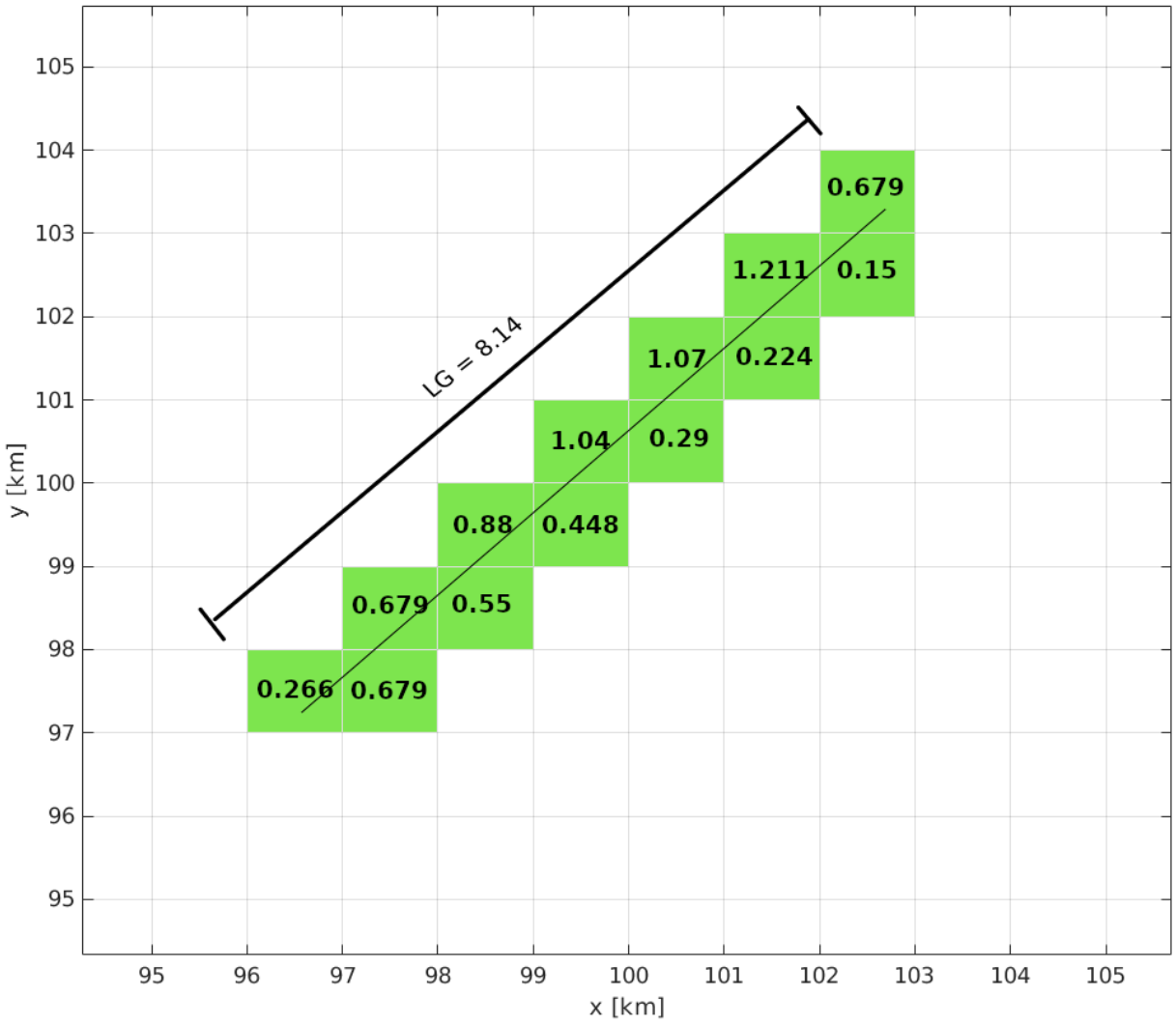

Figure 2.4: Non-zero values of the resulting distance matrix, containing the length of the portions of the link crossing those pixels.

With these two matrixes, γ_R and Δ_x, and a variable change, the integration along the slant path L can be evaluated with a discrete sum :

$$\begin{aligned} A &= \int_L \gamma_R \, dx \\ &= \int_{L_G} \gamma_R \, \frac{dx}{cos(\theta)} \\ &= \frac{1}{cos(\theta)} \sum_{i=1}^{N} \gamma_{Ri} \, \Delta_{xi} \end{aligned} \tag{2.6}$$

with θ the elevation angle, i indexing each pixel crossed by the ground path, γ_{Ri} the specific attenuation in this pixel and Δ_{xi} the distance traveled by the ground path in this pixel. In practice, the simulator calculates the element-by-element product of the two matrixes, and sums all the elements of the result : in fact, parts of the map where there is no rain have a 0 specific attenuation, and pixels that are not crossed have a 0 distance. The division by $cos(\theta)$ converts the result to the slant path.

2.4. Comparison of simulator results with lognormal probability density

A lognormal probability distribution is characterized by a density function as follows :

$$f_x(x|\mu,\sigma) = \frac{1}{x\sigma\sqrt{2\pi}} exp\left(\frac{-(logx-\mu)^2}{2\sigma^2}\right) \quad forx > 0 \tag{2.7}$$

Using Matlab's implementation of this distribution [17], it is possible to find μ and σ so that the complementary cumulative density function (CCDF) of the distribution fits the empirical CCDF (ECCDF) curve generated by the GSO attenuation results of the simulator. Figure 2.5 shows such a fit with the ECCDFs for 10° and 20° GSO elevation angles, at $f = 40GHz$ and $h_r = 3.36km$.

With $\mu = 1.7$ and $\sigma = 1.2$, a good fit for the 10° GSO elevation curve is obtained, whereas the 20° elevation ECCDF can be approximated with $\mu = 1.4$ and $\sigma = 1.05$. Such a fit can be obtained with every GSO elevation angle studied. The probabilities of exceedance of rain attenuation derived from the simulator results are thus well approximated by a log-normal distribution. As in literature, rain attenuation is generally known the behave as in a log-normal distribution [18], it shows the simulator is functioning properly, and its rain attenuation results are coherent.

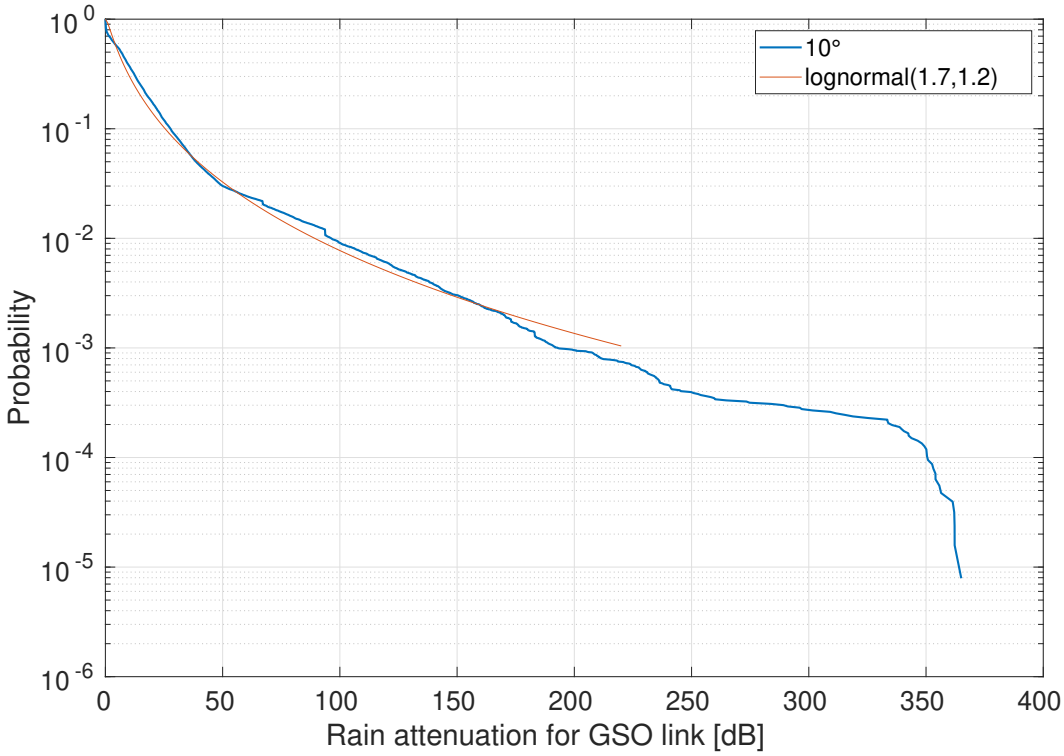

(a) 10° elevation angle

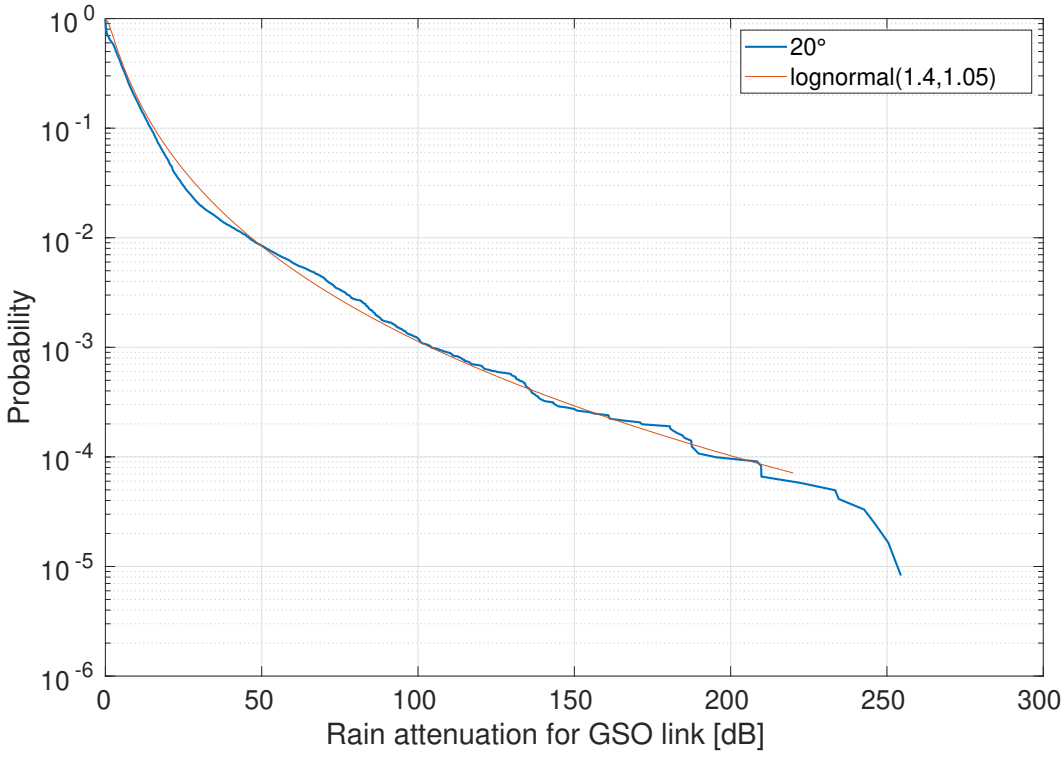

(b) 20° elevation angle

Figure 2.5: Comparison between empirical CCDF and lognormal fits, for $f = 40GHz$ and $h_r = 3.36km$.

3 | Results

3.1. Interference evaluation

As seen in Section 2.1.1, this work uses the C/I ratio as a metric to measure signal quality and impact of interference. Being a value defined for every time step of the simulation, C/I can be studied either by its evolution over time, with time series (which allows to check visually the correlation between C/I and other time-dependant variables), or in a probabilistic manner, using its complementary cumulative density function. Here, the latter method is used the most : by noting the decibel value of C/I for various probabilities of exceedance, and comparing those with the values obtained from other CCDF curves, it is possible to quantify the impact of a parameter on the quality of the signal received. Figure 3.1 shows a typical C/I CCDF curve, conditioned to having rain attenuation, for a GSO elevation angle of 30°, a link frequency of 40GHz, and a rain height calculated as recommended by the ITU-R.

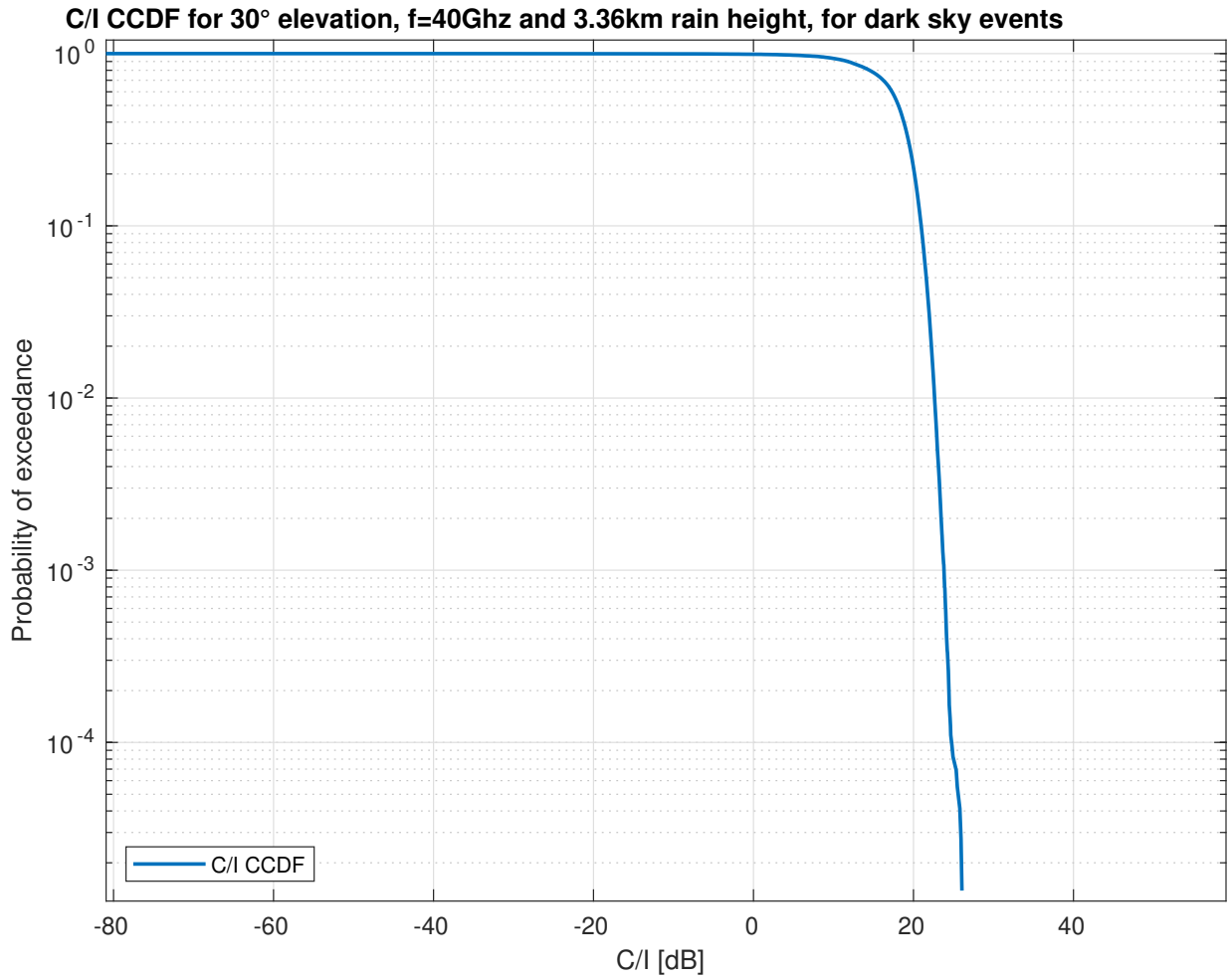

Figure 3.1: CCDF curve of C/I ratio, for $\theta = 30$, $f = 40GHz$, $h_r = 3.36km$.

3.2. Investigation of the dependence of the results on the GEO link parameters

Several parameters characterize a GSO-Earth link : in this work, four of them have been chosen to study the dependence of the C/I curves on such parameters. This section aims at illustrating these choices.

The first of these parameters is the **elevation angle** of the GSO link, θ. As satellites can be placed at various locations on the GEO belt, they can appear at different elevations when seen from the Earth. This has an impact on the length of the slant path of the link through the rain. This impact can be perceived both intuitively, by looking at the geometry of the event in Figure 1.3, or by considering the expression of the slant path,

Equation 1.6. For a fixed rain height, the length of the slant path is inversly proportionnal to $sin(\theta)$, meaning that the higher the elevation, the shorter the path through rain. As rain attenuation is a key effect in the problem studied here, it is interesting to study how the change in elevation angle will impact on the GSO signal.

A second parameter directly linked to rainfall is the **rain height** h_r. Just like the elevation angle, changing the rain height has a direct impact on the slant path, and thus on the intensity of rain attenuation. Rain height variation is linked to two real-life phenomena. The first is that ground stations positioned at different locations on the Earth will naturally have different rain height. The second is climate change. As average temperatures get generally warmer, the 0°C isotherm line raises : as an example, above London, the height of the 0°C isotherm has increased by nearly 200 meters between 1990 and 2010, which causes a significant increase in the rain height, and ultimately creates more rain attenuation on satellite links [19]. This change affects both the GSO and NGSO link : its effect on the C/I curves is thus not obvious.

The **frequency** f of the radiowave will also be studied as a variable. In the centimeter and millimeter ranges, rain attenuation increases considerably with frequency, following a power law [20] [21]. Satellites using different frequency bands will thus experience differently the atmospheric imparairments. Moreover, like the rain height, changing the frequency of both links will affect the quality of the signal at the receiver in non-trivial ways - it can therefore be an object of study.

Lastly, the number of NGSO satellites considered as interfering, *Nco* in short, is used as a variable. For this study, the intefering satellites will be selected as the VLEO satellites with the lowest separation angles above the avoidance angle threshold, which are the spacecrafts interacting the most with the geostationary system. The impact of the *Nco* on the intefering power gives clues on how much the VLEO satellites closest to the GSO-Earth link contribute to the interference.

In order to find a value for *Nco* suitable for the rest of the study, it is necessary to first consider it as a variable. Throughout the year simulated by the program, the maximum number of VLEO satellites visible by the ground station is 175. For this study, the chosen *Nco* are the powers of 2 from 2 to 64, providing a good variety of number of interfering satellites. The interfering power is calculated by summing the power received for each of the interfering satellites. The interfering spacecrafts are chosen by post processing the simulator output. For each interfering NGSO satellite at each timestamp, the simulator returns the power received from the GSO and NGSO link, the rain attenuation on both link, the separation angle and a flag that defines if rainfall occurs during the current event.

Here, only the VLEO satellites with the lowest separation angles over the avoidance angle threshold are kept, for each 30-second time step. Figure 3.2 shows a comparison of CCDF curves for varying *Nco*, at a GSO elevation angle of 30° and an avoidance angle of 2°.

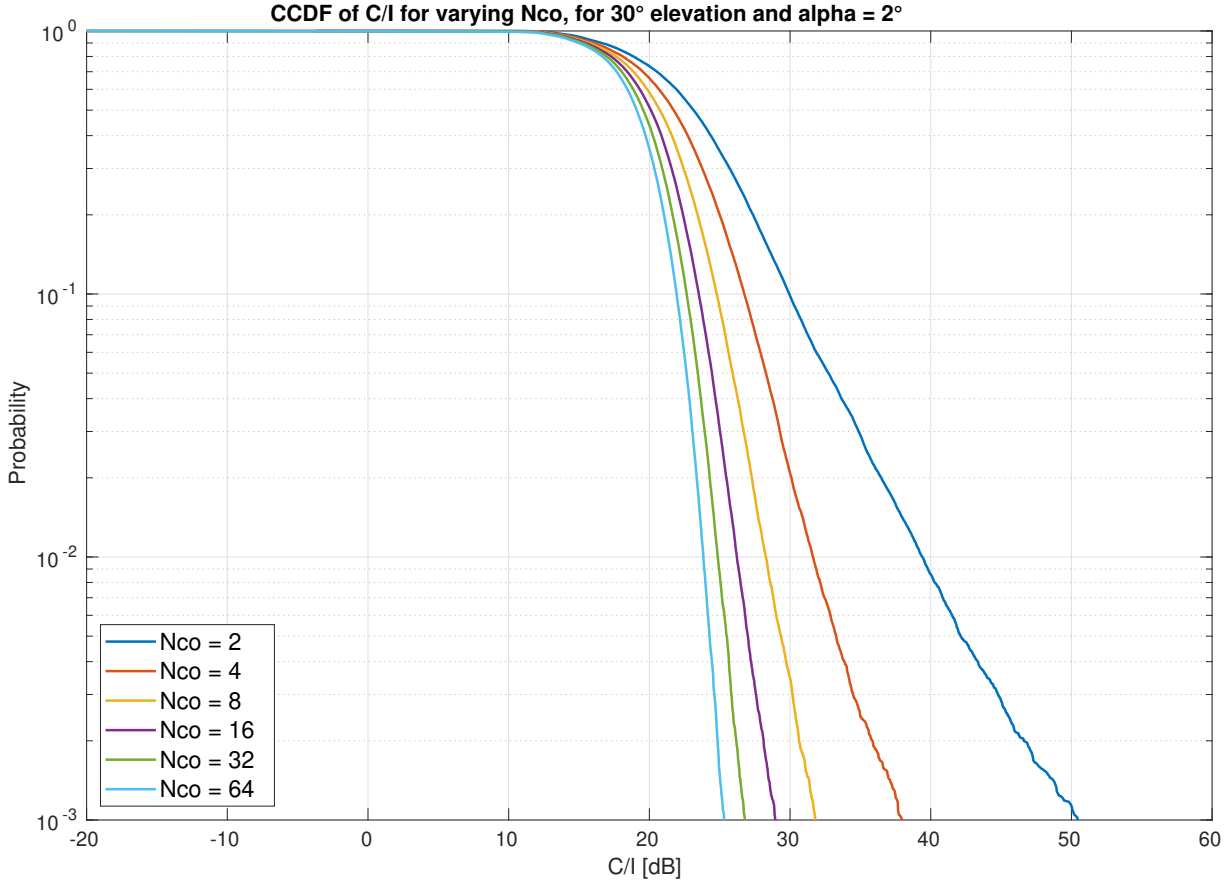

Figure 3.2: CCDF of C/I for varying Nco, 30° elevation.

As expected, a higher *Nco* results in more interference, and thus a lower C/I. However, a saturation effect is present : for the studied GSO elevation, the Nco = 16 and Nco = 64 curves are separated by 2 to 4 dB. Most of the interference is induced by the 8 to 16 satellites closest to the link. This justifies choosing Nco = 8 for the rest of the study, as this number is close to the saturation point, and represents a realistic case.

3.3. Investigation of the effect of GSO elevation angle

The elevation angles chosen for this study are the angles from 10° to 35°, with a step of 5°. This choice comes from three considerations :

- 10° is an elevation angle that guarantees visibility of the GSO satellite from the earth station.
- 35° is the multiple of 5 closest to the maximum elevation angle in the GEO satellites list used here.
- A step of 5 degrees has been chosen to reduce computation time, as each new elevation requires another run of the simulator. Limiting the study to 6 angles limits the time spent simulating.

With that choice made, it is possible to draw the CCDF curve for each of those elevation angles, conditioned on having rain attenuation, to compare them. Figure 3.3 shows these graphs.

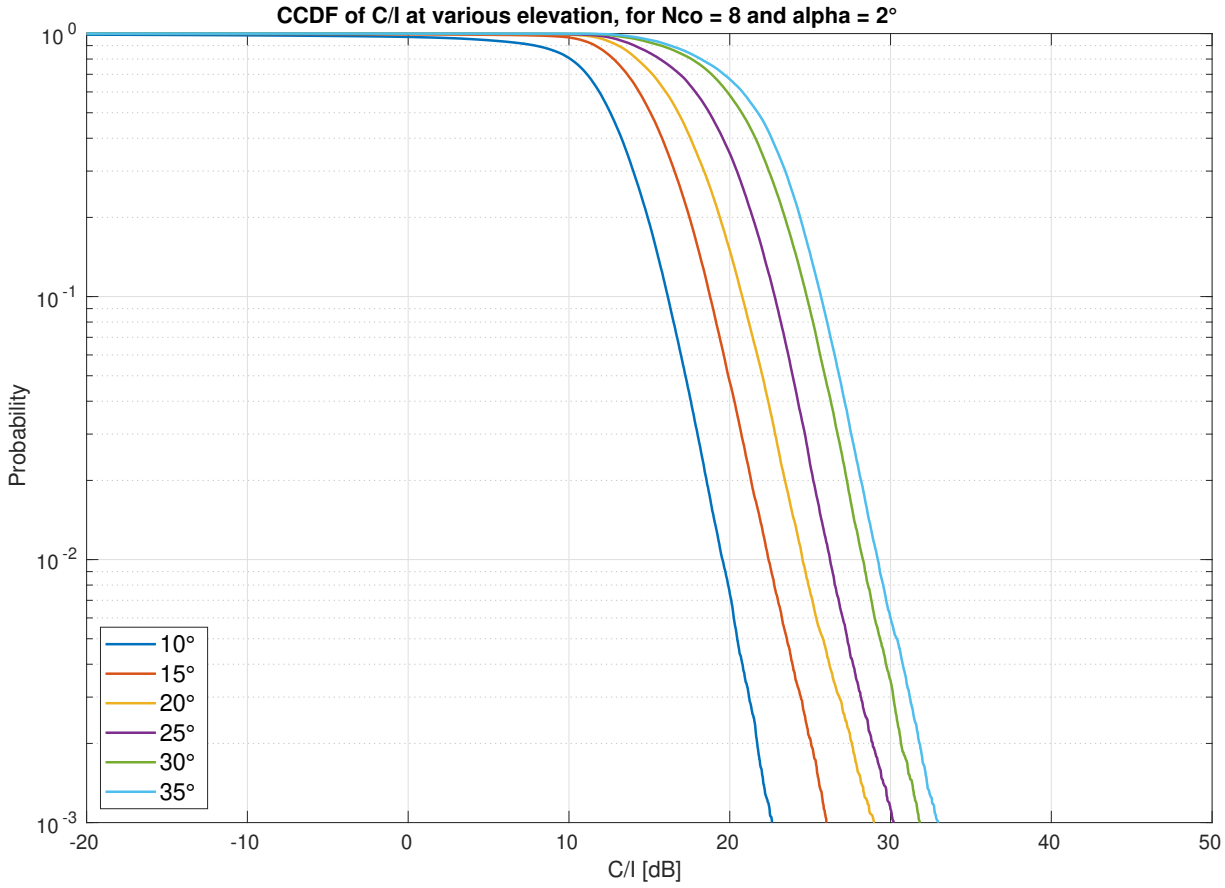

Figure 3.3: CCDF curves of C/I at various elevation, for Nco = 8 and $\alpha = 2$.

Several observations can be made on this plot. First, the 6 curves have very similar shapes, down to the 10^{-3} exceedance probability. The C/I ratio thus seems to behave in

Table 3.1: Table of C/I ratio [dB] for various elevation angle, and various probabilities of exceedance.

Probability \ Elevation	10°	15°	20°	25°	30°	35°
0.5	12.55	15.06	16.82	18.77	20.73	21.71
0.2	14.88	17.49	19.32	21.42	23.41	24.38
0.1	16.13	18.77	20.77	22.78	24.79	25.66
0.05	17.23	19.9	22.03	23.92	25.92	26.81
0.01	19.54	22.4	24.52	26.22	28.28	29.21
0.005	20.4	23.55	25.8	27.3	29.34	30.4

a similar fashion whatever the GSO satellite's elevation . However, a clear shift in C/I happens when the elevation angle changes. The C/I ratio decreases as the elevation angle decreases, in an almost regular way between the angles of 10° and 30°. The 35° curve is very close to the 30° one. In order to quantify these observations, Table 3.1 contains the decibel values of C/I for various probabilities of exceedance.

In the 15° to 30° range for the elevation, the shift in decibel values for the C/I is **approximately 2 dB for 5° of elevation change**. The 10° curve is 2.5 dB below the 15° curve, and the 35° degree curve 1 dB above the 30° one.

The decrease in C/I ratio is a consequence of the increase in rain attenuation on the GSO link. As the GSO elevation angle decreases, the path of the link through rain gets longer, thus experiencing more attenuation. This attenuation of the desired signal is reflected on the CCDFs of C, as shown in Figure 3.4. The GSO signal received is thus weaker for lower elevation : as the I signal, the NGSO one, is not affected by the change in GSO elevation angle, the resulting C/I ratio is lower.

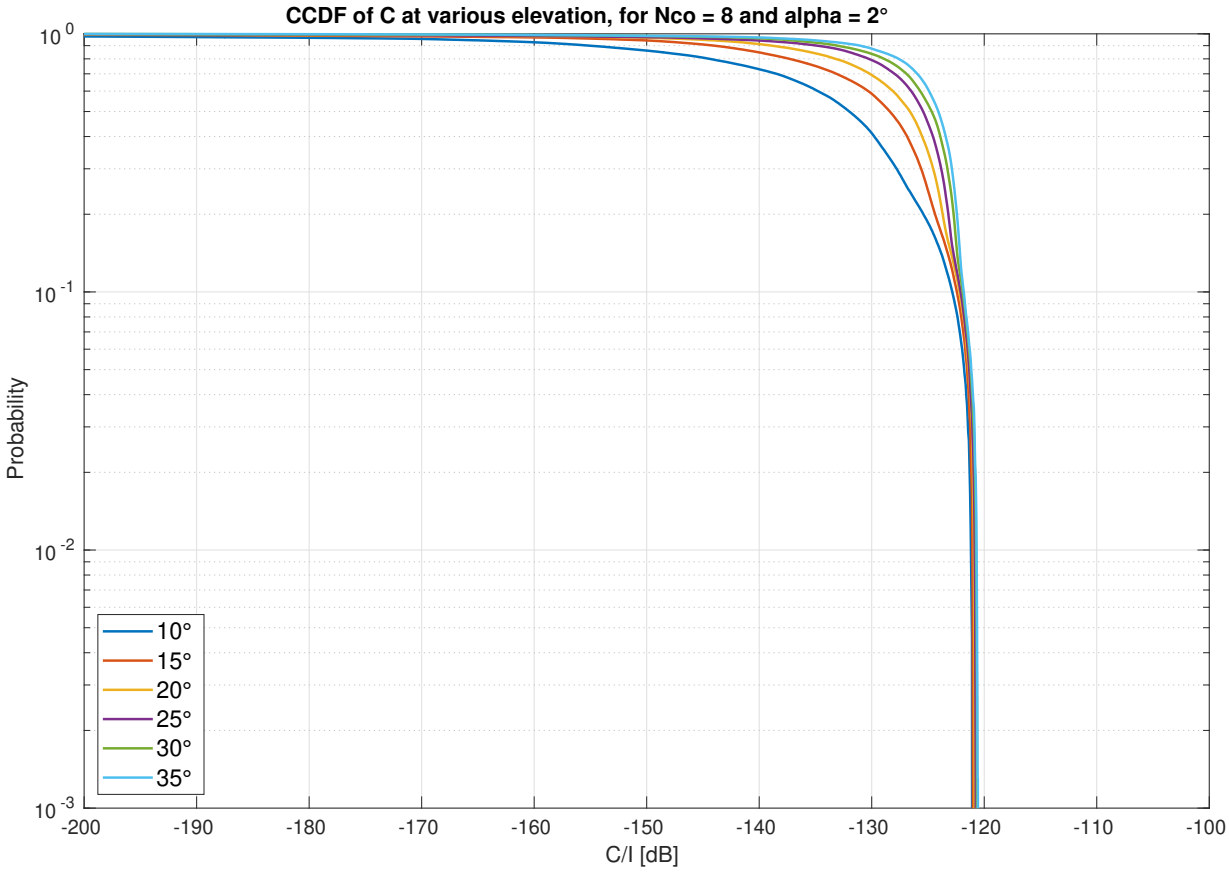

Figure 3.4: CCDF curves of C at various elevation angles.

3.4. Investigation of the effect of rain height variations

For rain height, the three values considered here are 2.36km, 3.36km and 4.36km. 3.36km is the rain height described by recommandation ITU-R P.839-4 for the location of the ground station. As the change in rain height affects the rain attenuation on both links, the resulting variation in C/I ratio is expected to be small. Therefore, the values of 2.36km and 4.36km have been chosen to try and obtain a visible effect on the C/I CCDF curves. Figure 3.5 shows the C/I CCDF curves for all three rain heights at 30° GSO elevation.

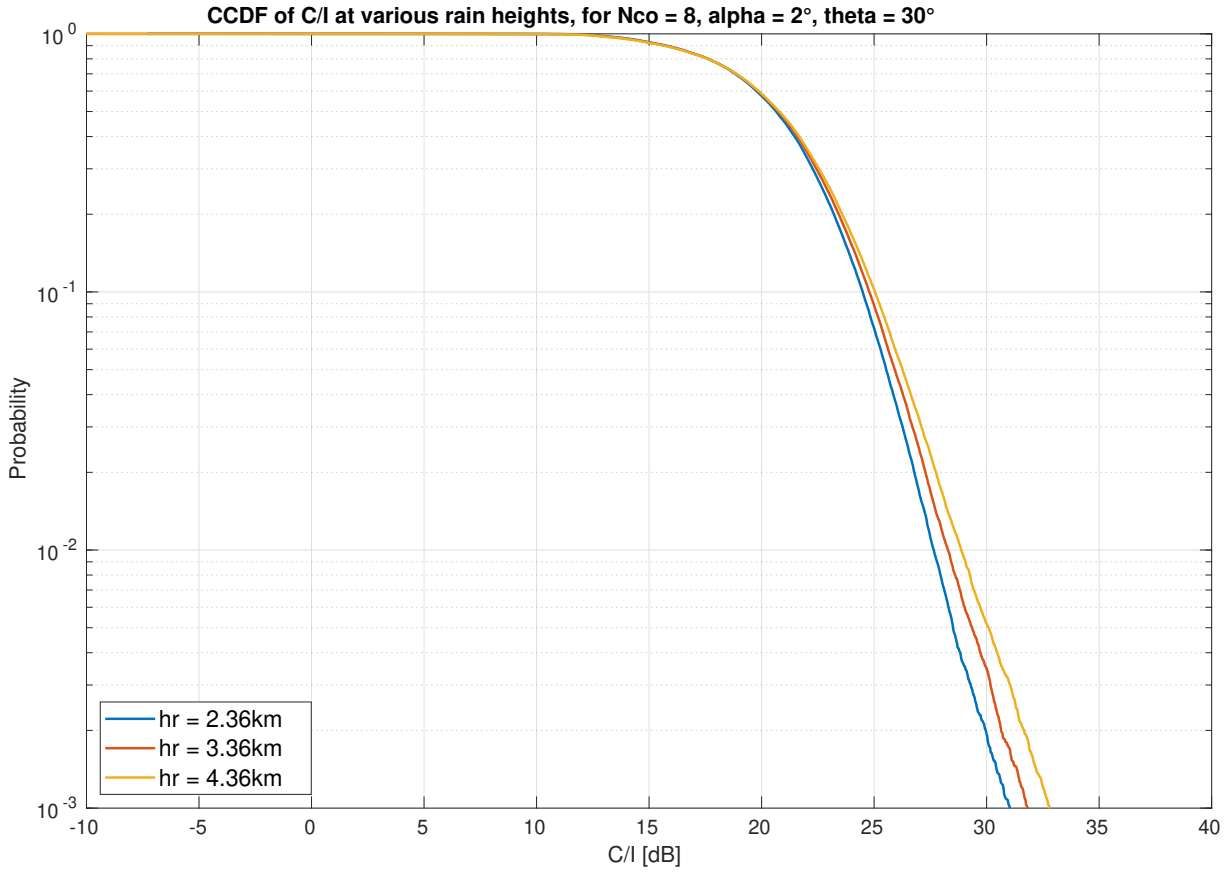

Figure 3.5: CCDF curves of C/I at various rain heights, for Nco = 8, $\alpha = 2$ and 30° elevation angle.

All three curves are very similar, and are only separated by a maximum of 2 dB. For this GSO elevation, the highest rain height, corresponding to the highest rain attenuation, results in the highest C/I ratio. The interfering signal is thus the most affected by the change in rain height and by the consequent increase in rain attenuation : **the effect is however very limited**.

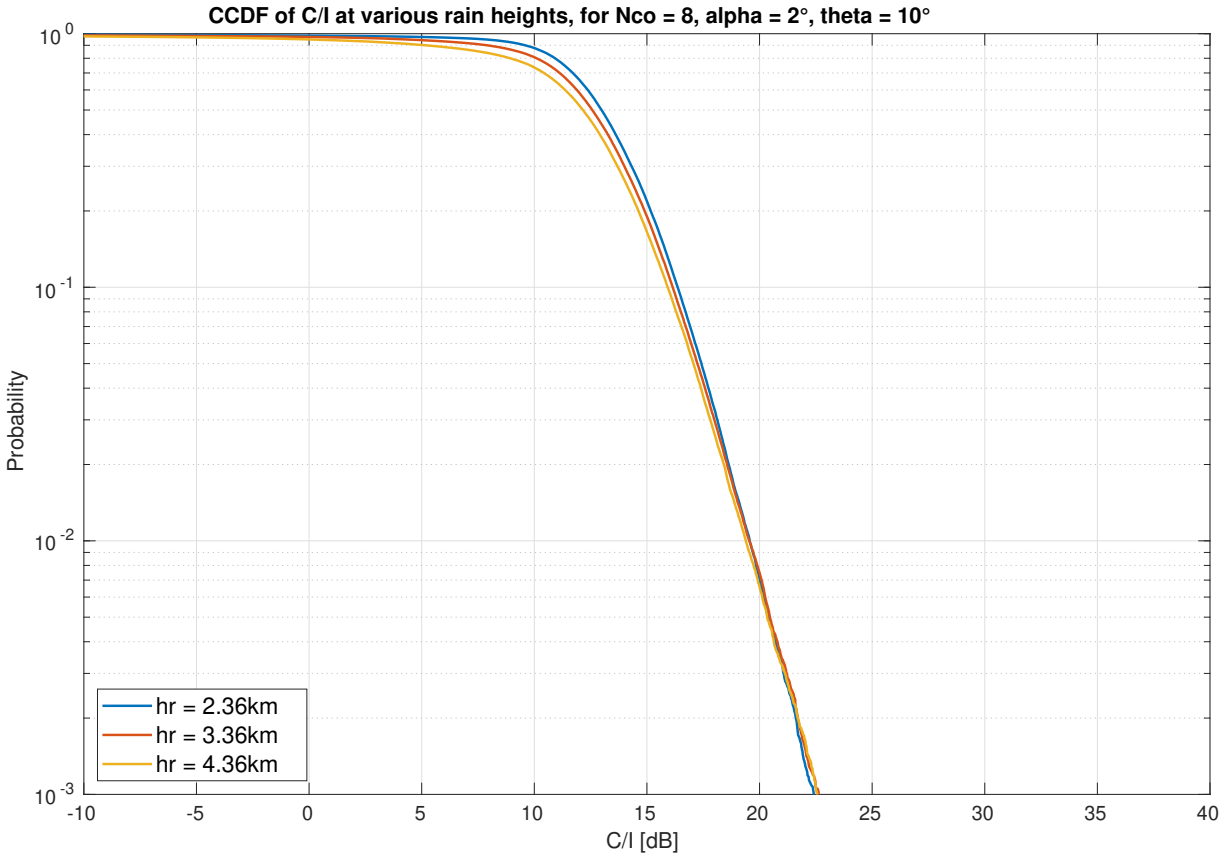

Figure 3.6: CCDF curves of C/I at various rain heights, for Nco = 8, $\alpha = 2$ and 10° elevation angle.

However, at lower GSO elevation angles, the behaviour is different, as shown in Figure 3.6. At 10° elevation angle, the lower the rain height, the higher the C/I ratio. The smaller elevation induces a longer path through the rain for the GSO-Earth link : the increase in rain height therefore has a significant effect on the desired signal, whereas the interfering one is less impacted. The effect of the change in rain height on C/I ratio thus depends on the elevation angle of the GSO link.

3.5. Study of the effects of frequency change

For link frequency, two values have been chosen, 20 GHz and 40 GHz. This allows the comparison between the C/I ratio in the Ku-band and in the Ka-band. The changes in frequency are applied to both links. Figure 3.7 shows the two C/I CCDF curves for *Nco* = 8, $\alpha = 2°$ and at a 30° GSO elevation angle.

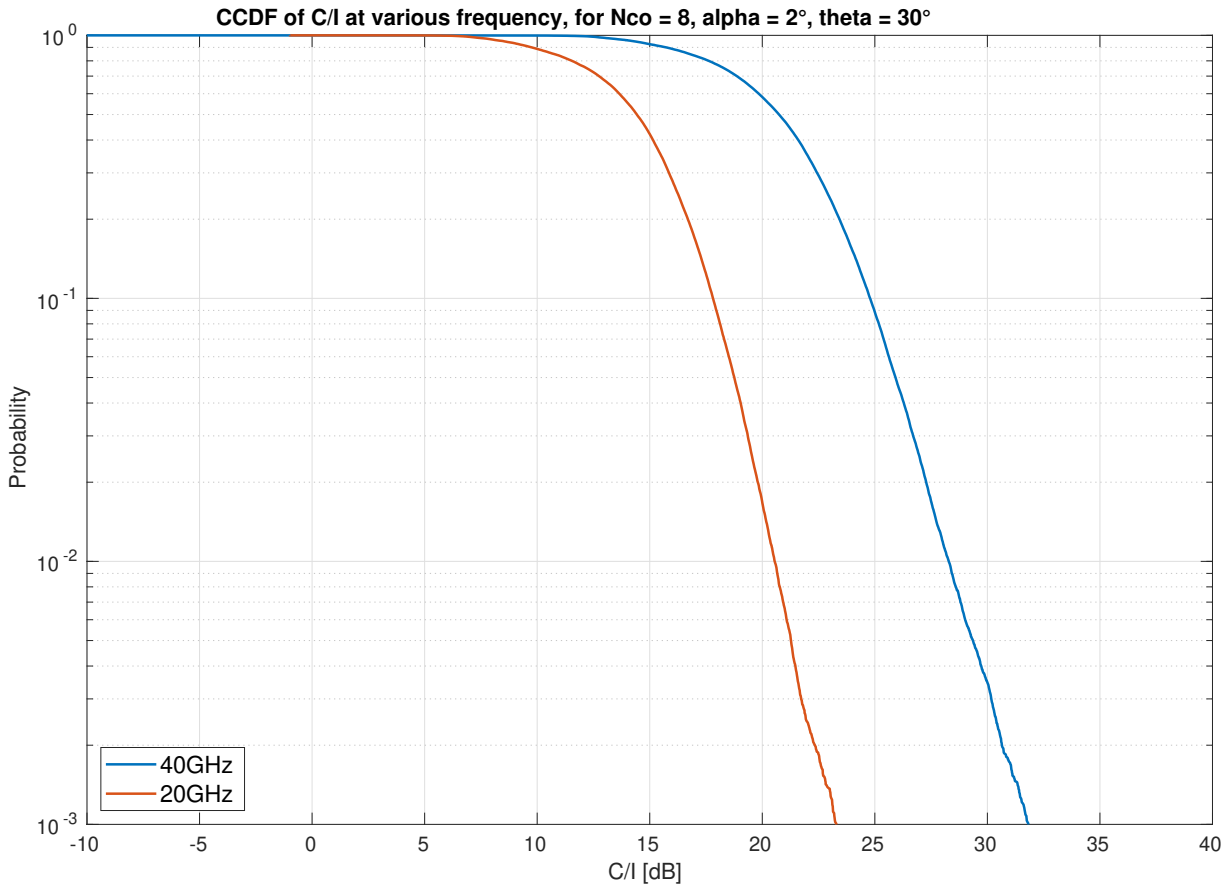

Figure 3.7: CCDF curves of C/I at various frequencies, for Nco = 8, $\alpha = 2°$ and 30° elevation angle.

The graph shows **a higher C/I ratio for the 40 GHz case, compared to the 20 GHz one**. The difference is significant : 7 dB for the 0.1 probability of exceedance, and 8 dB for the 0.01 probability. Both the magnitude of the difference, and the fact that the 40 GHz link has a better C/I, are direct consequences of the effect of the frequency change on the NGSO link. Figure 3.8 shows the CCDF curves of interfering signal power for both frequencies.

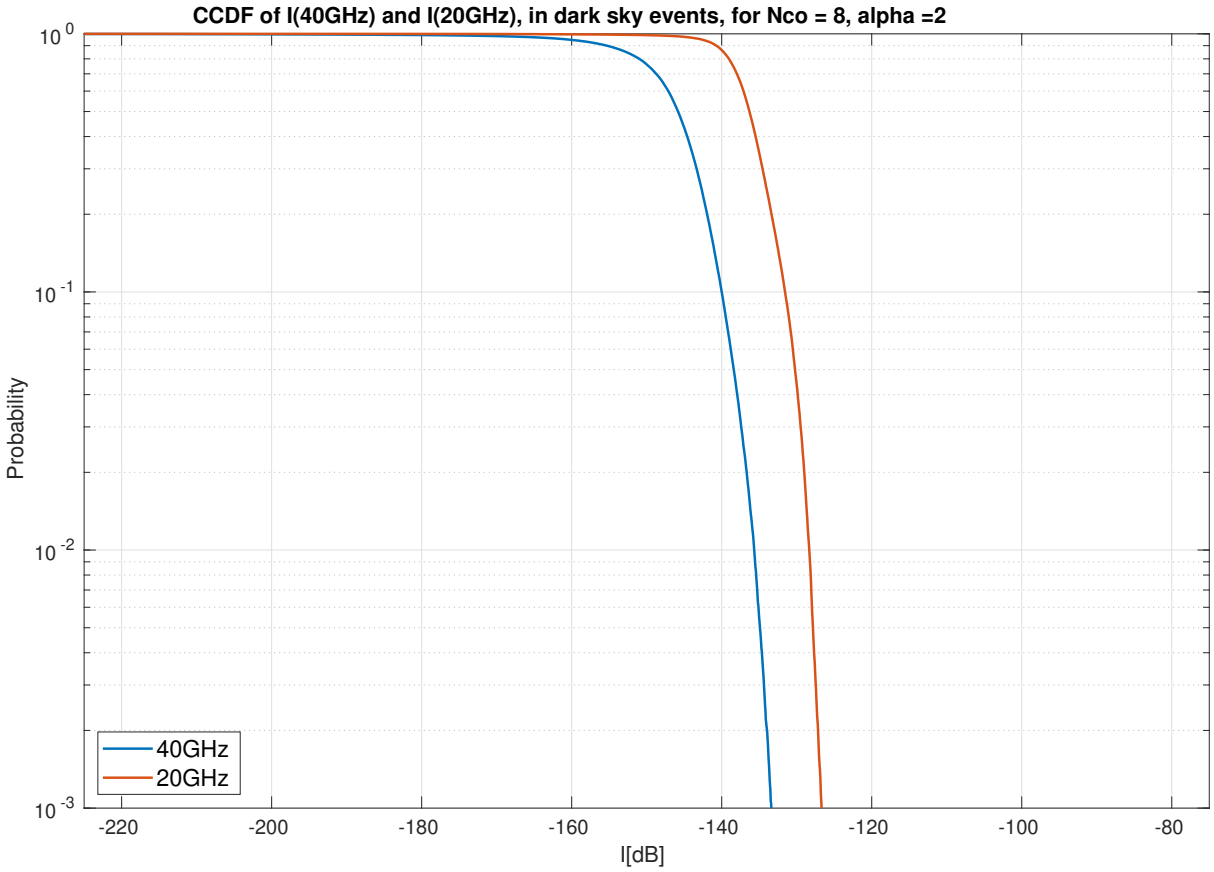

Figure 3.8: CCDF of I at various frequencies, for Nco = 8, $\alpha = 2$ and 30° elevation angle.

The NGSO links have a lower rain attenuation at 20 GHz than at 40 GHz. As the decrease in rain attenuation at the lower frequency affects all NGSO links individually, and the total power of the I signal is the sum of the power budget of all NGSO links, the difference between the two curves is significant. Indeed, the two CCDF curves for the I signal appear to be shifted by an almost constant value of about 10 dB. It is noteworthy to compare this value with the shift in the curves of C, the GSO signal power.

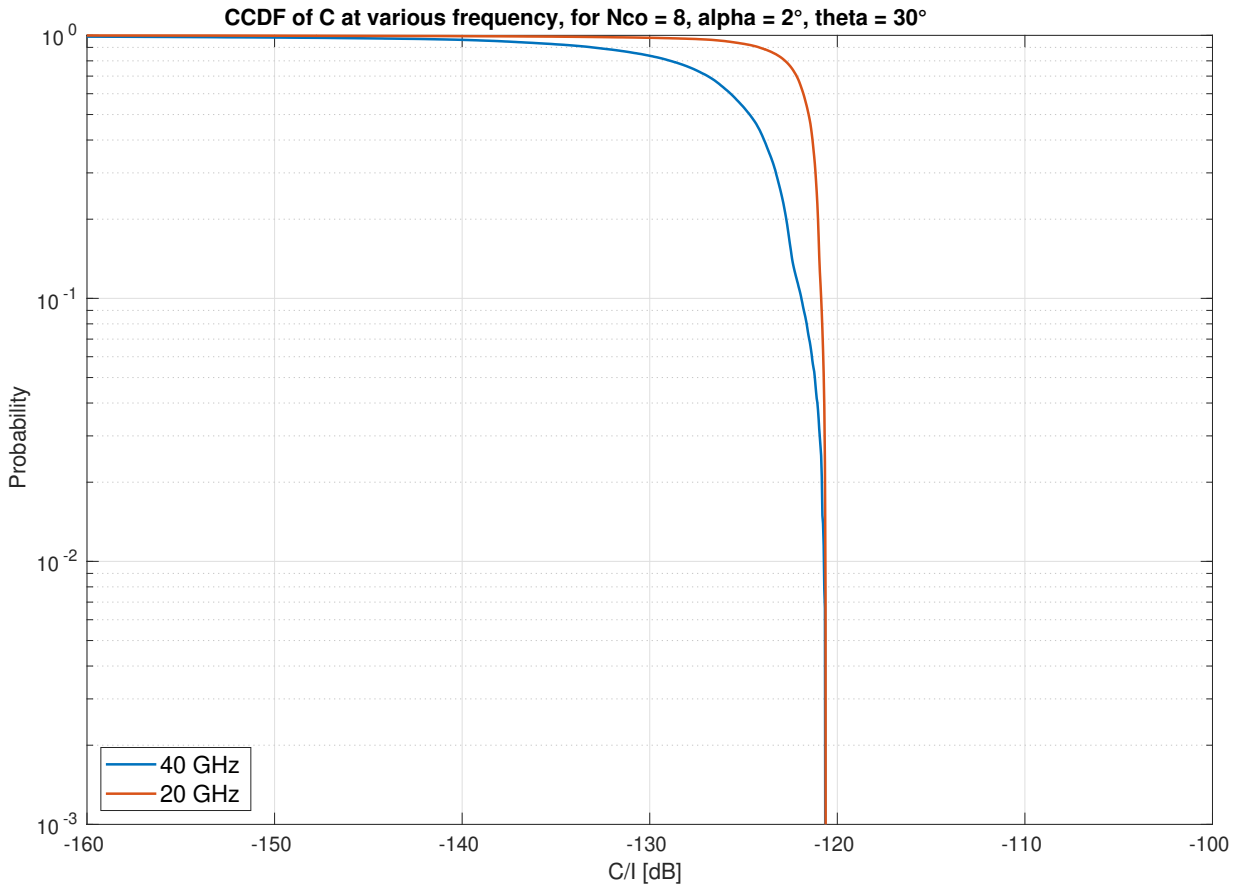

Figure 3.9: CCDF of C at various frequencies, for 30° elevation angle.

In both cases, the received power is lower in the 40 GHz case. Despite this, both curves have the same maximum value : this happens because the receiver gain of the ground antenna is tuned according to frequency, thus the gain is lower in the 20 GHz case. In total, as shown in Figure 3.9, the difference between the C curves is less significant than between the I curves. The difference in C/I ratio curves is thus **caused by the lower interfering power received in the 40 GHz case**, which is itself induced by the higher rain attenuation on each NGSO link, ultimately resulting in a lower total contribution for the I signal.

3.6. Correlation analysis

A key element that can be extracted from the simulator is the correlation between the GSO rain attenuation and NGSO one: not only this highly affects the C/I, but, in addition, this is a key piece of information for analytical approaches aimed at modeling the interference

issue discussed in this work. One method to study the correlation between the two rain attenuations is the use of intensity plots.

These plots can be understood as heat maps of the data. Each $[Att_{rain,GSO}, Att_{rain,NGSO}]$ couple is placed into a bin. A bin is the set of couples where $Att_{rain,GSO}$ and $Att_{rain,NGSO}$ fall into specific intervals. Each pixel of the intensity plot represents one of these bins : the color of the pixel is linked to the number of couples in the bin, red indicating a high density and blue a low density. The plots of Figure 3.10 are created with bins of 0.1 dB width, with $Nco = 8$ and $\alpha = 2°$. With these values of Nco and avoidance angle, it is expected to obtain a correlation : a low avoidance angle implies that the VLEO satellites can emit from a position very close to the GSO-Earth link, and in this implementation the 8 satellite with closest separation angle to the avoidance angle threshold are selected as the ones causing interference. Since the NGSO-Earth links are characterized by a narrow angular separation from the main beam between the GSO satellite and the Earth station, those paths are likely to cross the same rain field, and consequently to experience a similar rain attenuation.

Another method to study the correlation between two data sets is evaluating their *Pearson's correlation coefficient*. Pearson's correlation coefficient ρ is a measure of the linear correlation between the two sets, and is calculated as follows :

$$\rho = \frac{\sum_{i=1}^{n}(x_i - \bar{x})(y_i - \bar{y})}{\sqrt{\sum_{i=1}^{n}(x_i - \bar{x})^2}\sqrt{\sum_{i=1}^{n}(y_i - \bar{y})^2}} \tag{3.1}$$

where x and y are datasets with n elements each, and $\bar{x}$, $\bar{y}$ are their mean. ρ has a value between -1 and 1 : -1 indicates a perfect negative linear anticorrelation, 0 indicates no linear correlation, and 1 indicates a perfect linear correlation. Using Matlab's implementation of Pearson's correlation coefficient [22], and using both rain attenuations in dB as the tested datasets, Table 3.2 has been obtained, containing ρ for each tested GSO elevation angle.

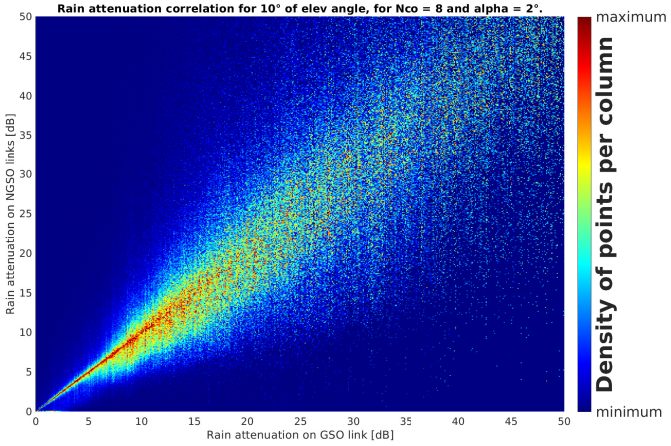

(a) 10° elevation angle

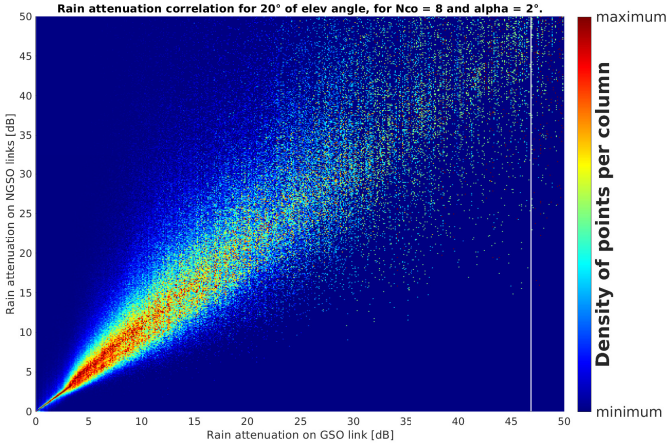

(b) 20° elevation angle

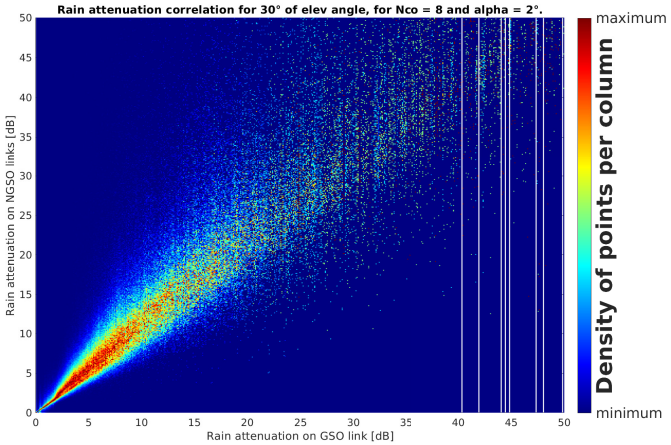

(c) 30° elevation angle

Figure 3.10: Correlation between GSO rain attenuation and NGSO rain attenuation at various elevation angles, for $\alpha = 2$.

Table 3.2: Table of Pearson's correlation coefficient between GSO and NGSO rain attenuations, for $\alpha = 2°$.

Elevation angle	10°	15°	20°	25°	30°	35°
ρ	0.8905	0.8642	0.8928	0.9129	0.9142	0.9325

Throughout all GSO elevation angles, the intensity plots shown in Figure 3.10 show that **the GSO rain attenuation and NGSO rain attenuation are well correlated** : the points of higher density are located close to the $y = x$ line, indicating a relationship similar to a linear one. This correlation is the strongest for lower rain attenuations : beyond about 20 dB, the data is sparser, revealing weaker correlation at high rain attenuations. For the linear correlation coefficients, all values are above 0.85, indicating a strong overall linear correlation between the two datasets.

To further study this correlation, the rain attenuation for the GSO and NGSO links respectively was modeled in two ways : **fully correlated** ($\rho = 1$) and **fully uncorrelated** ($\rho = 0$). The C/I ratios curves that result from these two methods can be compared with the results from the simulator. In order to do this, the fully correlated and uncorrelated models have been implemented as follows :

- for the correlated model, the GSO rain attenuation is calculated as described in Section 2.3.2. The rain attenuation for all NGSO links is set equal to the GSO attenuation.
- for the uncorrelated model : by carrying out simulations over a full year, enough data has been obtained to define the empirical CDF of both the GSO and NGSO rain attenuations. At each time step, samples of rain attenuation for either paths are randomly extracted from such CDFs, so as to preserve the long-term statistics.

Using these calculations, the CCDF curves of C/I in Figure 3.11 have been obtained. At both 10° and 30° elevation, the result with simulated GSO and NGSO rain attenuations resembles the C/I ratio behaviour derived through the fully correlated model. This is a consequence of the strong observed correlation between the attenuations.

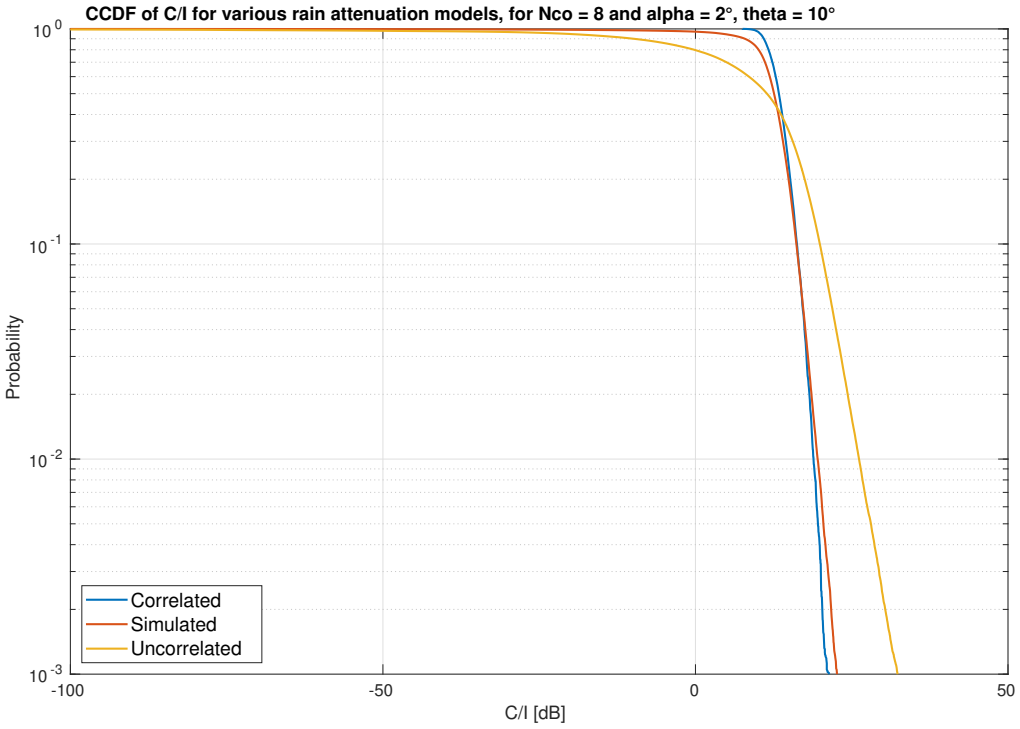

(a) 10° elevation angle

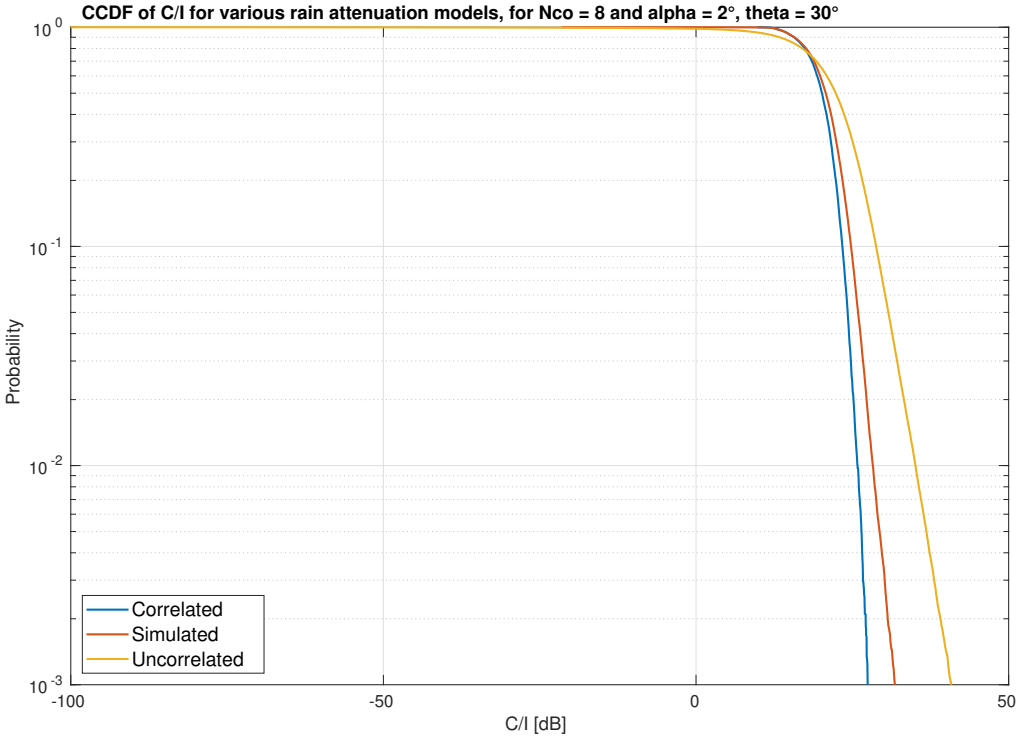

(b) 30° elevation angle

Figure 3.11: CCDF curves of C/I for correlated, simulated and uncorrelated models, Nco = 8, $\alpha = 2°$

To evaluate the dependence of the correlation on avoidance angle, it is interesting to study the case of a larger α, here chosen as 20°. As the interfering satellites will be further from the GSO beam, the correlation between $Att_{rain,GSO}$ and $Att_{rain,NGSO}$ is expected to be weaker. Figure 3.12 shows intensity plots for this case, and Table 3.3 the correlation coefficients.

Table 3.3: Table of Pearson's correlation coefficient between GSO and NGSO rain attenuation, for $\alpha = 20°$.

Elevation angle	10°	15°	20°	25°	30°	35°
ρ	0.6872	0.6515	0.6259	0.6666	0.6526	0.7714

These results clearly show a weaker correlation between the rain attenuation variables for $\alpha = 20°$ than for $\alpha = 2°$. Intensity plots are sparser in the 20° case, and regions of higher density deviate significantly from the $y = x$ line. This is especially apparent in the 20° GSO elevation case, where high density pixels seem to be located along two distinct lines. At 30° GSO elevation, NGSO rain attenuations appear to be twice as much as the GSO attenuation ones. These plots also show sparser data beyond 20 dB attenuation. As for correlation coefficients, they are significantly lower in the $\alpha = 20°$ case than in the $\alpha = 2°$ one, again denoting weaker correlation.

To further demonstrate the reduced correlation, CCDF curves of C/I ratio for the three aforementioned models have been plotted, and are shown in Figure 3.13. At 30° elevation, the curve resulting from the correlated model, and the one resulting from simulation data are completely apart. The fully-correlated model can not be used to accurately describe NGSO rain attenuation in this case. Compared with the C/I CCDF curves at $\alpha = 2°$ (Figure 3.11), the curves of Figure 3.13 show a weaker correlation. This sample result clearly points out how the use of simplified models of the correlation between the GSO and NGSO attenuations can seldom offer accurate results.

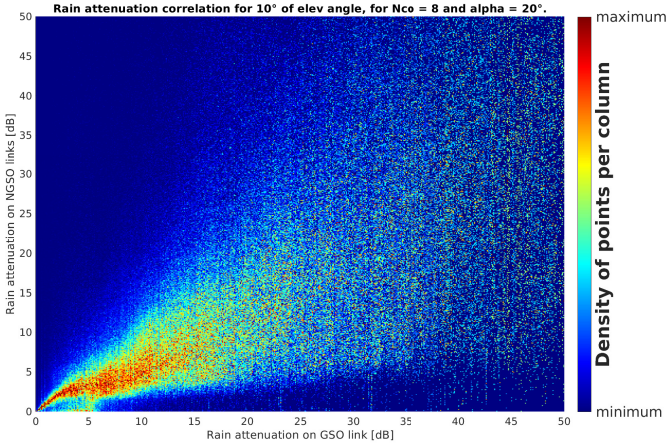

(a) 10° elevation angle

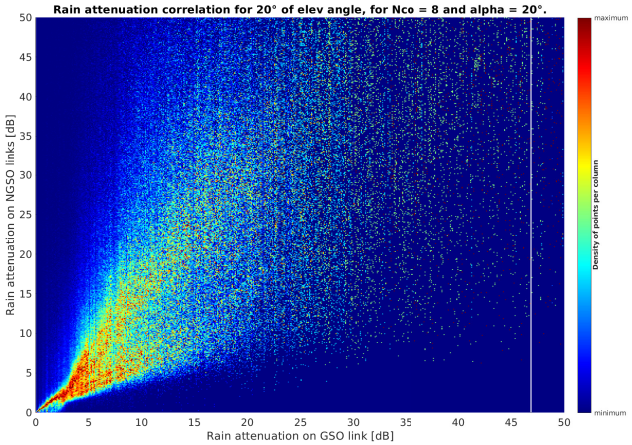

(b) 20° elevation angle

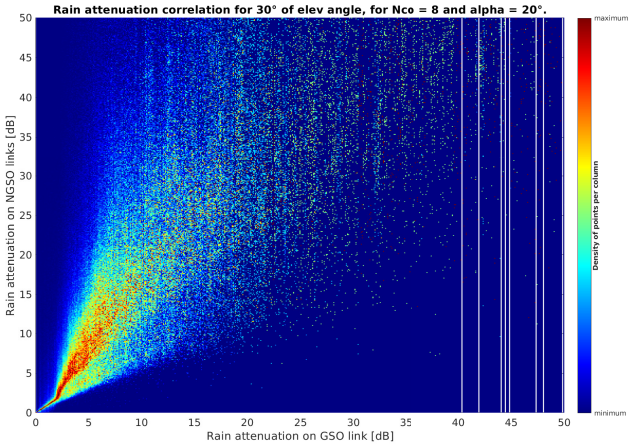

(c) 30° elevation angle

Figure 3.12: Correlation between GSO rain attenuation and NGSO rain attenuation at various GSO elevation angles, for $\alpha = 20°$.

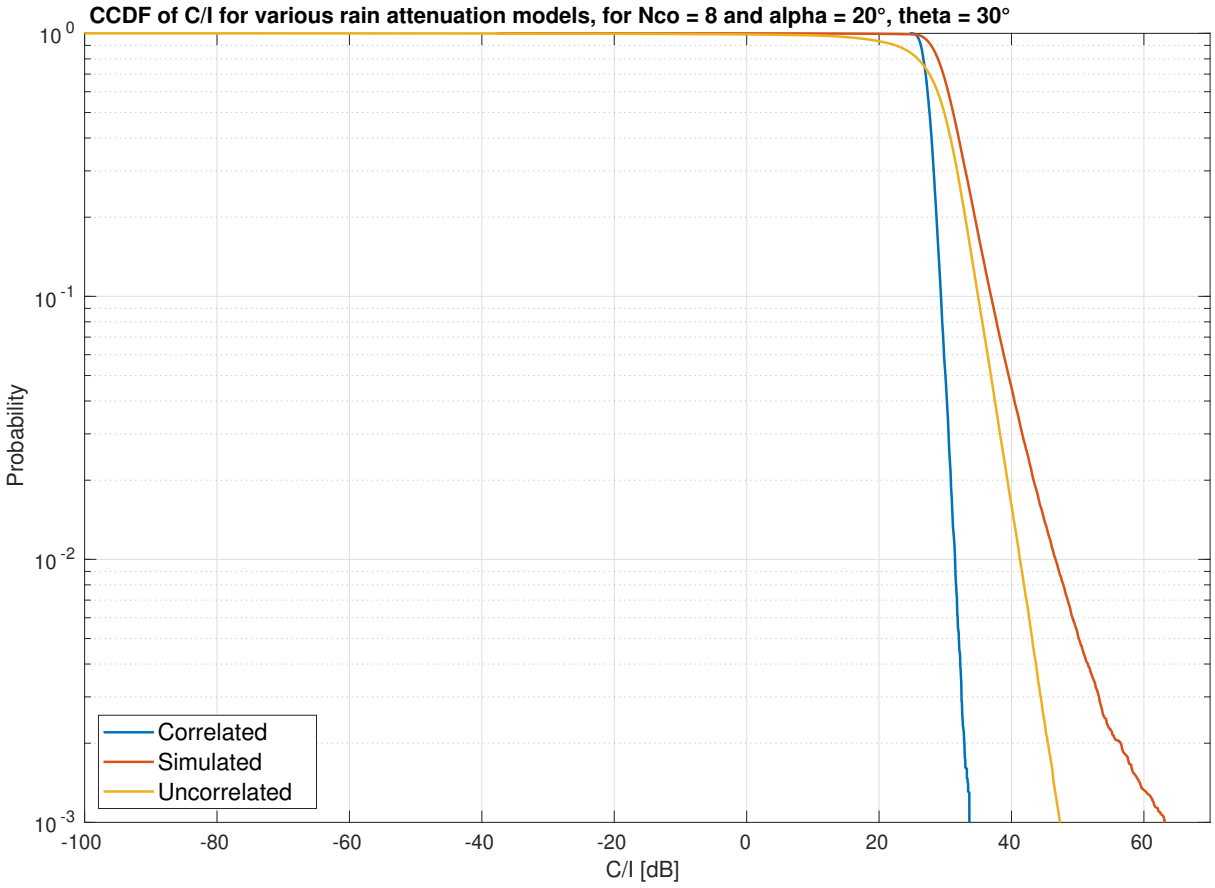

Figure 3.13: CCDF curves of C/I for correlated, simulated and uncorrelated models, Nco = 8, $\alpha = 20°$, 30° GSO elevation angle.

In order to study a wider range of avoidance angles, Pearson's correlation coefficient can be calculated on a larger number of data sets. Figure 3.14 shows the variation of ρ as a function of the avoidance angle, for values of α between 0° and 50°, for all the considered GSO elevation angles.

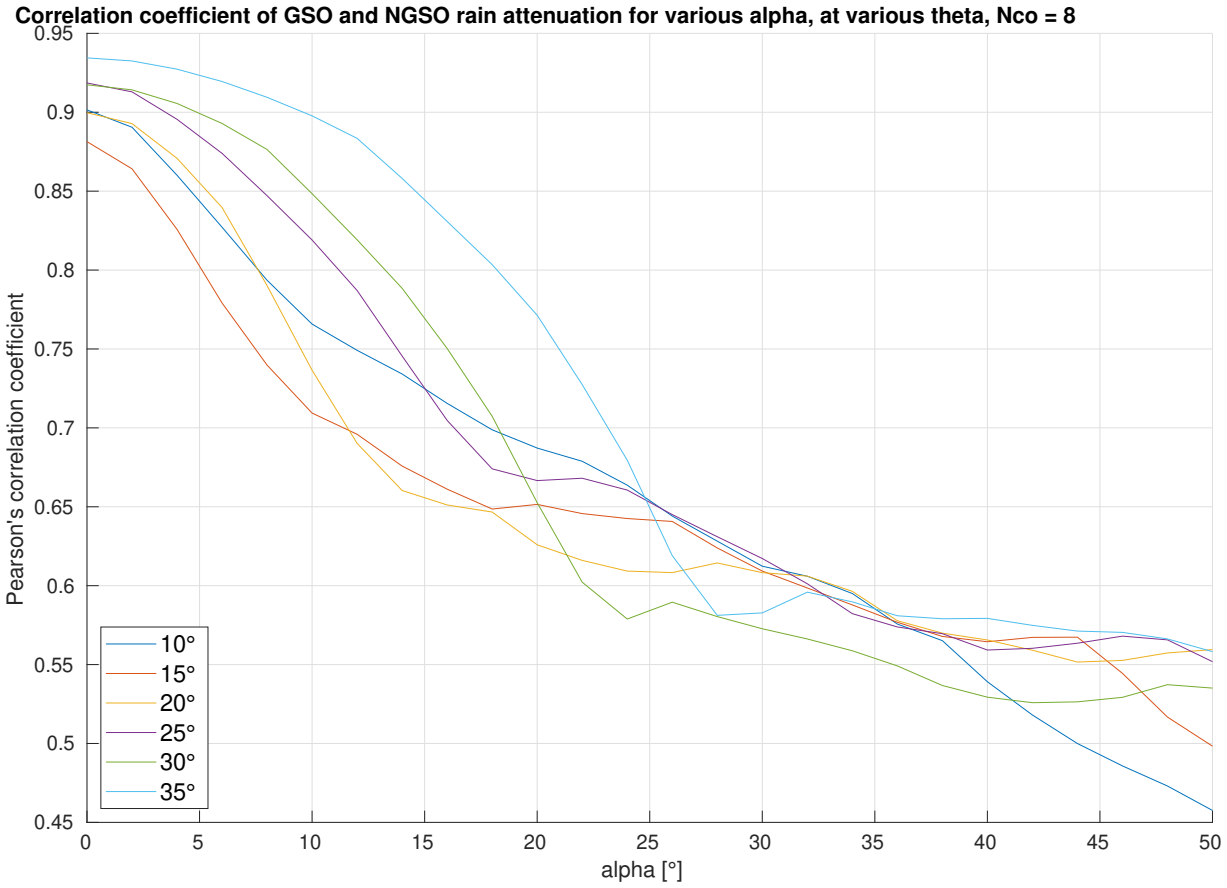

Figure 3.14: Linear correlation coeffcient between rain attenuations, at various avoidance angles and various elevation angles.

Several observations can be made on this figure : as expected, the correlation coefficent decreases when the avoidance angle increases, for all elevation angles. How much it decreases depends on the GSO elevation angle, with lower elevations seeing a steeper decline and a generally lower ρ. Beyond an avoidance angle of 20° to 25°, the coefficient decreases in a more regular trend, with differences between elevation angles greatly reduced.

At $\alpha = 2°$, both the direct correlation analysis between the two rain attenuations, and the comparison between C/I CCDF curves seem to indicate that a correlation exists between GSO rain attenuation and NGSO rain attenuation. Indeed, both methods of analysis have shown a link between the two attenuations, and the model closest to the simulations in terms of C/I is the fully-correlated one. The fully-correlated model can be used as a satisfactory approximation to obtain the CCDF curves of C/I. This correlation is only observed to some extent : the data becomes sparse in the intensity plots beyond 20 dB,

and the CCDF curve of the simulated result does not overlap perfectly with the one of the fully-correlated model. Moreover, the strength of the correlation directly depends on the avoidance angle threshold. This is shown both by the study of the $\alpha = 20°$ case, that demonstrates a weaker correlation than in the $\alpha = 2°$ case, and by the linear correlation coefficient decreasing fast as the avoidance angle increases. In this case, the correlated model cannot be used to approximate NGSO rain attenuation. This result confirms our exceptations : indeed, at growing values of α, the NGSO satellites are less likely to experience the same rain fields the GSO link does. Lastly, at avoidance angles below 20°, higher elevations seem to show stronger correlations between GSO rain attenuation and NGSO rain attenuation.

4 | Conclusions and future work

The number of VLEO satellites has been quickly increasing over the last few years, and this trend is expected to continue in the near future. As this population grows, so does the interference induced by the constellations on GSO links. This is especially true as the frequencies used by VLEO constellations are shared with geostationary systems. At these frequencies, the most detrimental atmospheric impairment for the radio waves is rain attenuation. Given the variety of parameters characterizing GSO to Earth links, it is noteworthy to analyse how the impact of the interference induced by NGSO constellations varies with the most relevant system variables. This thesis analyses various scenarios of interference, mainly according to three system parameters : the GSO elevation angle, rain height and frequency. Moreover, this work also studies the correlation between GSO and NGSO rain attenuation.

This analysis has been conducted using a model implemented by software, aimed at evaluating these interferences by simulating GSO and NGSO links over a duration of one year, taking into account rain attenuation, the most significant among the atmospheric impairments. Using the C/I ratio as a metric to measure the amount of interferences, the study has yielded results for the effects of all three characteristics. For the elevation angle, higher GSO elevations result in better signal quality, with the CCDF curves of C/I shifting in a consistent fashion for lower elevations. Variations in rain height have shown to weakly impact the C/I ratio. Higher frequencies result in higher C/I ratios, with the difference being quite significant : this is caused by the interfering signal being strongly affected by the increased experienced rain attenuation. Correlation analysis has shown that GSO rain attenuation and NGSO rain attenuation are strongly correlated at low avoidance angles and low attenuation values; the correlation becomes weaker at higher avoidance angle thresholds.

Among the possible atmospheric impairments, only the rain attenuation is taken into account by the model. Future studies could include attenuations induced by gases and clouds, in order to analyse more comprehensive scenarios. The analysis of additional link parameters could also be of interest. A study of the performance of the system through

a metric other than C/I, for example throughput, could be conducted. Further analysis of the correlation between GSO and NGSO rain attenuation could also be conducted, in particular on possible analytical models linking the two attenuations. This analysis could be conducted for various avoidance angle thresholds, in order to discern the best model that can obtained for each case.

Bibliography

[1] Union of Concerned Scientists (UCS). *UCS Satellite Database*. `https://www.ucsusa.org/resources/satellite-database`. [Online, accessed 04-October-2023], 2023.

[2] Alexandra Witze. *2022 was a record year for space launches*. `https://www.nature.com/articles/d41586-023-00048-7`. [Online, accessed 04-October-2023], 2023.

[3] Enrico Polo. *Model to investigate the interference induced by NGSO constellations on GSO system ground stations*. Master's thesis, Politecnico Di Milano, 2022.

[4] Orbits and Kepler's Laws. `https://science.nasa.gov/resource/orbits-and-keplers-laws/`. [Online, accessed 16-October-2023], 2023.

[5] Louis J. Ippolito Jr. *Satellite Communications Systems Engineering: Atmospheric Effects, Satellite Link Design and System Performance*. Wiley, 2008.

[6] ITU-R. *Specific attenuation model for rain for use in prediction methods*. Recommendation P.838-3. 2005.

[7] ITU-R. *Rain height model for prediction methods*. Recommendation P.839-4. 2013.

[8] ITU-R. *Propagation data and prediction methods required for the design of Earth-space telecommunication systems*. Recommendation P.618-14. 2023.

[9] C. Capsoni, F. Fedi, A. Paraboni, A. Pawlina. *Data and theory for a new model of the horizontal structure of rain cells for propagation applications*. *Radio Science*, 22, No. 3:395–404, May-June 1987.

[10] Lorenzo Luini and Carlo Capsoni. *MultiEXCELL: A New Rain Field Model for Propagation Applications*. *IEEE Transactions on Antennas and Propagation*, Vol. 22, No. 3, November 2011.

[11] Lorenzo Luini. *Modeling the Space-Time Evolution of Rain Fields : Electromagnetic wave propagation applications*. 2020.

[12] *SpaceX V-Band Non-Geostationary Satellite System: Attachment A, Technical Information to Supplement Schedule S.* Technical Report SAT-LOA-20170301-00027, FCC, 2016.

[13] ITU-R. *Application of Article 22 of the Radio Regulations to the protection of geostationary fixed-satellite service and broadcasting-satellite service networks from non-geostationary fixed-satellite service systems in the frequency bands 37.5-39.5 GHz, 39.5-42.5 GHz, 47.2-50.2 GHz and 50.4-51.4 GHz.* Resolution 770. 2019.

[14] ITU-R. *Radiation diagrams for use as design objectives for antennas of earth stations operating with geostationary satellites.* Recommendation P.580-6. 2004.

[15] ITU-R. *Protection of geostationary fixed-satellite service, broadcasting-satellite service and mobile-satellite service networks from the aggregate interference produced by multiple non-geostationary fixed-satellite service systems in the frequency bands 37.5-39.5 GHz, 39.5-42.5 GHz, 47.2-50.2 GHz and 50.4-51.4 GHz.*Resolution 769 (WRC-19). 2019.

[16] FCC. *Implementation of the Final Acts of the 2019 World Radiocommunication Conference. Federal Register, 2023-09-29*, 2023.

[17] Matlab. *Lognormal probability density function*, `https://it.mathworks.com/help/stats/lognpdf.html`. [Online, accessed 25-October-2023].

[18] ITU-R. *Time series synthesis of tropospheric impairments.* Recommandation P1853-2. 2019.

[19] A. Al-Mreri K. Paulson. *Trends in the incidence of rain height and the effects on global satellite telecommunications. IET Microwaves, Antennas & Propgation*, 2010.

[20] D. W. Blood R. K. Crane. *Handbook for the estimation of microwave propagation effects - link calculations for earth-space paths.* Technical report, NASA Goddard Space Flight Center, 1979.

[21] W. L. Stutzman J. D. Laster. *Frequency scaling of rain attenuation for satellite communication links. IEEE Transactions on Antennas and Propagation, Vol. 43, Issue 11*, 1995.

[22] Matlab. *Correlation coefficients.* `https://it.mathworks.com/help/matlab/ref/corrcoef.html` [Online, accessed 9-november-2023].

List of Figures

List of Tables

List of Symbols

Variable	Description	SI unit
$\boldsymbol{e}$	Eccentricity	
$\boldsymbol{i}$	Inclination	degree
$\boldsymbol{\gamma_R}$	Specific attenuation	dB/km
$\boldsymbol{h_r}$	Rain height	km
$\boldsymbol{\theta}$	Elevation angle	degree
$\boldsymbol{R}$	Rain rate	mm/h
$\boldsymbol{Att_{Rain,GSO}}$	Rain attenuation on GSO link	dB
$\boldsymbol{Att_{Rain,NGSO}}$	Rain attenuation on NGSO link	dB
$\boldsymbol{\alpha}$	Avoidance angle threshold	degree
$\boldsymbol{\Delta_x}$	Distance matrix	
$\boldsymbol{f}$	Link frequency	GHz
$\boldsymbol{Nco}$	Number of satellites considered as interfering	
$\boldsymbol{\rho}$	Pearson's correlation coefficient	

Acknowledgements

First of all, I would like to thank Prof. Lorenzo Luini and Enrico Polo for their guidance throughout the project. Their help, their availability, and their patience during the whole thesis have been precious.

Merci à mes parents pour leur soutien sans faille, sans lequel rien n'aurait été possible.

Merci à Lucie pour sa bienveillance précieuse durant toute cette période.

Merci à Christophe, Lucie, Léonie et tous mes amis de Polimi, qui ont navigué avec moi dans les eaux parfois mouvementées de la vie et des études à l'étranger.